ATLAS NSW Alignment System Radiation Tolerance

Senior Thesis

Presented to
Faculty of the School of Arts and Sciences
Brandeis University

Undergraduate Program in Physics

In partial fulfillment of the requirements for the degree of
Bachelor of Science

by
Michael MacKenzie

Advisor:
James Bensinger

Waltham, MA, May 2016

Signatures

James Bensinger Ph.D., Committee Member	Date
Craig Blocker Ph.D., Committee Member	Date

Acknowledgements

I would like to thank my thesis advisor, James Bensinger, for his constant support throughout this project. I would also like to thank Kevan Hashemi and Richard Studley for their mentorship and leadership in the HEP lab. Lastly, I would like to thank Camila Pazos and Benjamin Hechtman for their assistance.

Abstract

The ATLAS project at CERN detects emergent particles after high-energy proton-proton collisions. For accurate measurements of particle locations, the detector systems must utilize an accurate alignment system. Brandeis High Energy Physics department, or Brandeis HEP, has been critical in the creation of the alignment system in the muon spectrometer at ATLAS. Currently, Brandeis HEP has been working on an alignment system for the New Small Wheel, or NSW, which is an upgrade to replace the current Small Wheel in the ATLAS detector. The NSW will have to endure a greater amount of cavern radiation due to a higher luminosity delivered by the LHC. This paper describes the ionizing radiation and neutron radiation tolerance of the currently being designed and built alignment system for the NSW. This paper shows that the current design will have a safety factor of 3.7 to simultaneous ionizing radiation and neutron radiation, while having a safety factor of 14 to ionizing radiation and a safety factor of 5 to neutron radiation separately.

1 Background

The Large Hadron Collider, or LHC, at CERN is capable of accelerating particles to near light speed, utilizing superconducting magnets to guide the particles in an ultrahigh vacuum tube. ATLAS and CMS are the general-purpose detectors at the LHC.[1] The ATLAS project at CERN collides two high-energy protons in order to study the resultant particles created by the interaction.

From the high-energy collision of two protons, ATLAS then determines each particle emerging from the event, and each particle's momentum and energy using sophisticated detectors. ATLAS is composed of four main components to analyze the emergent particles: the inner detector, the calorimeter, the muon spectrometer, and the magnetic system. The first three are detectors, while the last is used to bend charged particles so the other components can analyze the particles' momenta.[2] The inner detector is used to measure emergent charged particles' momenta.[3] The calorimeter is used to measure the energy of both charged and neutral particles by absorbing their energy. The only particles that emerge from the calorimeter are neutrinos, which we cannot measure, and muons, which are typically high energy and have a much larger mass than the similar electron so are not absorbed by the calorimeter.[4] An image of the entire detector is shown in figure 1.

In order to measure muons, ATLAS uses an entire detector system specifically to find them and measure their momenta. This detector system is called the muon spectrometer. The muon has the same charge as an electron, but the ratio of the muon mass to the electron mass is 207 which causes the need for the larger detector system to determine its momentum. The magnetic field created by ATLAS bends the muon much less than the electron, so the large muon spectrometer allows the measurement of the muon momentum to the required accuracy of the detection system.[6]

The muon detector is composed of four sections to measure the location of muons. The four sections are disks perpendicular to the beam line, often called "wheels." Each wheel has large trapezoidal wedges, composed of chambers, creating a disk, and smaller wedges behind them forming a disk that covers the separations between the large wedges. This forms a complete and gapless disk that is the wheel. An image of a wheel design is shown in figure

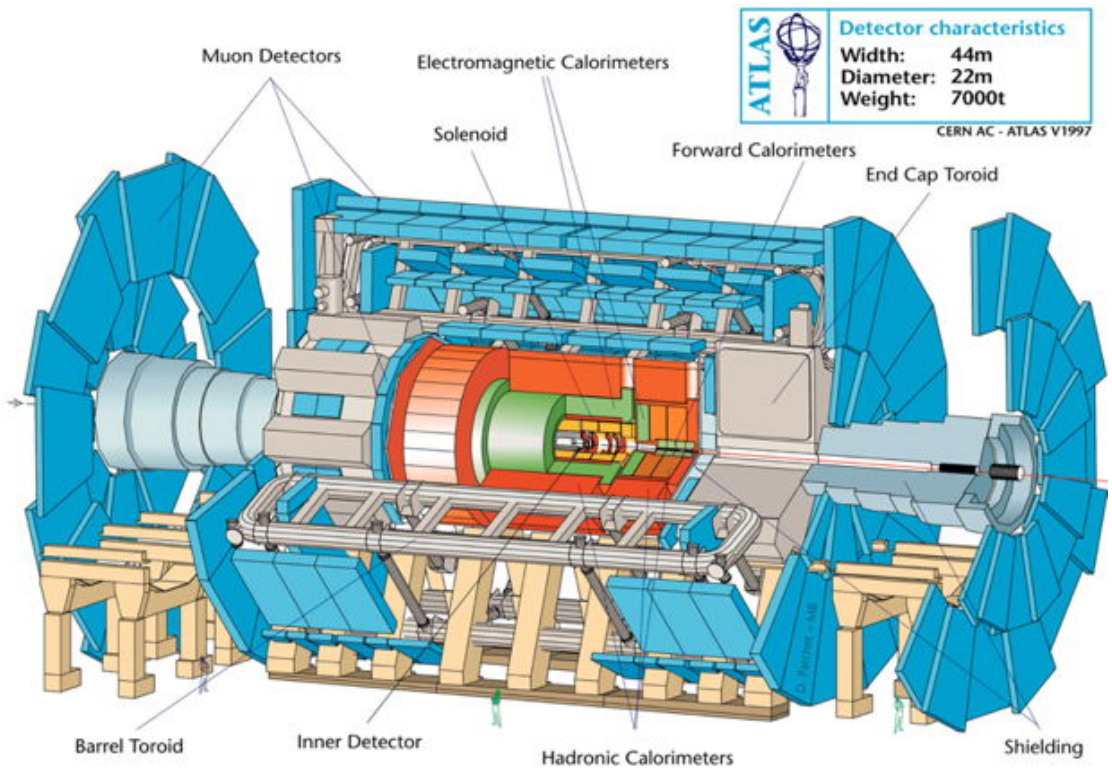

Figure 1: *Pictured is a drawing of the ATLAS detector. It shows the inner detector, the calorimeters, the muon spectrometer, and the magnetic systems.[5]*

2. In the image, there are shown the two overlapping disks of trapezoids forming the gapless disk that is the wheel. The four wheels from closest to the interaction point to farthest are the Small Wheel, the EE, the Big Wheel, and the HO. The four wheels each detect the location of a muon that passes through it, which is bent by the magnetic field created by ATLAS between the Small Wheel and the Big Wheel. The bending of a charged particle in a known magnetic field gives the momentum of that charged particle. A straight line of the particle's path is determined from the interaction point to the Small Wheel and from the Big Wheel to the HO, so that the bending of the particle between the Small Wheel and the Big Wheel can be measured as the "sagitta" of the particle, or the peak difference between the curved path the particle took and the straight line between the points it intersected in the Small Wheel and Big Wheel. The muons have such a high momentum, that they only bend $1 - 2mm$ over the entire muon spectrometer. The goal of the spectrometer is to measure the muon's sagitta to 10%, which requires the overall accuracy of the spectrometer to be at worst $100\mu m$.[6]

The chambers that form the wheels are the actual detectors. The wheels are composed of both sTGCs, which stands for small-strip Thin Gap Chambers, and resistive strip Micromegas. These two chambers measure the location of a muon traveling through the chamber to an accuracy greater than $100\mu m$.[8] This accuracy is only to the location of the muon's path within the chamber, and not the system as a whole. To know where the location of the chamber is in relation to the global coordinate system in the muon spectrometer, ATLAS

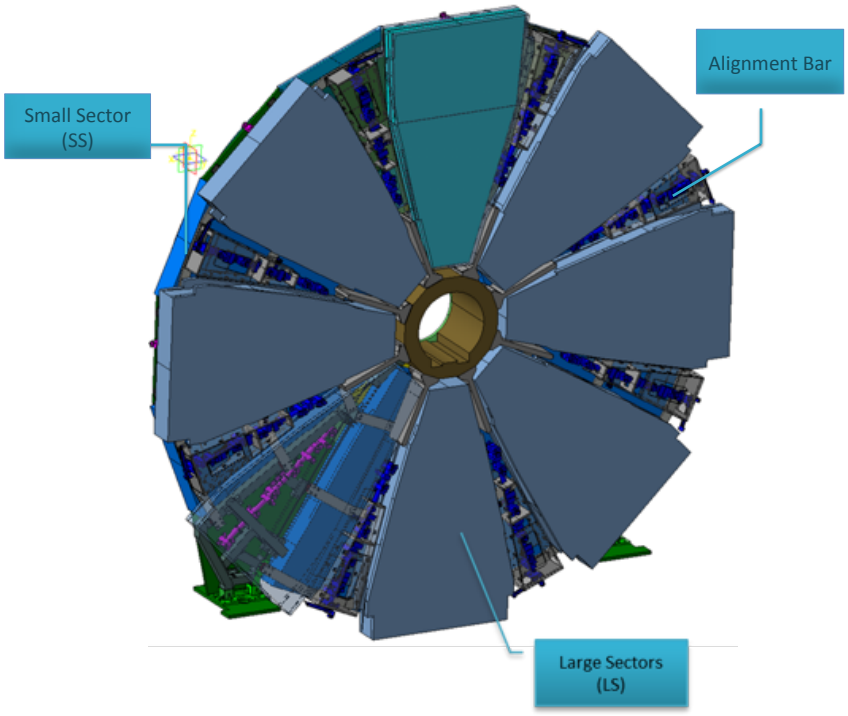

Figure 2: *Pictured is a drawing of the New Small Wheel.[7] It is composed of two disks of trapezoidal wedges overlapped to form a gapless disk. Each wedge is composed of chambers which detect muons that travel through them.*

uses a sophisticated alignment system. To maintain the system's accuracy, the alignment system must have an accuracy greater than $100\mu m$.[6]

The LHC is being upgraded to supply a luminosity of $5 * 10^{34} cm^{-2} s^{-1}$[8]. This high luminosity creates a high cavern background radiation due to interactions creating particle showers. The ionizing radiation environment in ATLAS is shown in figure 3 and the neutron radiation environment is shown in figure 4. The increase in the luminosity can be then accounted for and added to the environment to predict the increased background. A graph of total accumulated dose over 10 years in the location of the Small Wheel after the upgrade is shown in figure 5. The increase in cavern background requires that the current Small Wheel be upgraded to handle this total radiation for the next ten years.[9] The upgraded wheel is called the New Small Wheel, or NSW, and is currently being designed and built. This upgrade also requires an upgrade to the alignment system used in the current Small Wheel. The alignment system for the NSW must still have an accuracy of greater than $100\mu m$, be able to withstand the increased luminosity, and be able to be integrated with the alignment system being used in the rest of the muon spectrometer.

2 Alignment System

The alignment system is designed to create a coordinate system that can be incorporated with the ATLAS and LHC coordinate systems, and to know the location and shape of each

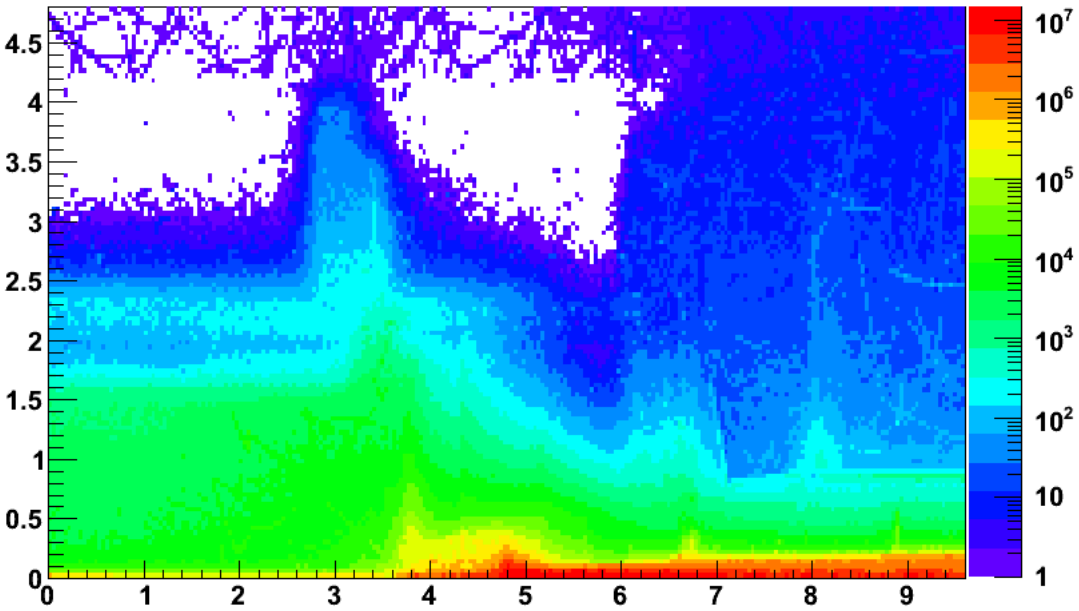

Figure 3: *This graph shows the simulated flux of photons in* $kHz * cm^{-2}$ *in ATLAS. The horizontal axis is the z-axis in ATLAS, or the distance along the beam line from the interaction point, and the vertical axis is the radius from the beam line. This assumes a beam energy of* $14TeV$ *but only a luminosity of* $10^{34}cm^{-2}s^{-1}$*.[9]*

of the chambers in the muon spectrometer. To do this, ATLAS uses "alignment bars," which act as rulers in the spectrometer. The alignment bars are well measured before and during installation, and then their deformation is tracked throughout their lifetime in ATLAS.[10]

The alignment bars are like spokes in each of the wheels, running in the same plane as the wheel and perpendicular to the beam line. Currently there are sixteen bars in each wheel. The bars are able to locate each other, and this system is over-determined so that it creates a well known grid in the wheel. Each wheel grid is then combined in a web by the bars in each wheel locating the bars in the other wheels. This creates a global coordinate system for the muon spectrometer. This coordinate system is then connected to the LHC coordinate system by viewing "monuments" in the cavern whose locations are accurately known. In this way, the alignment system is able to determine absolute locations instead of relative locations.[10]

Utilizing the global coordinate system, the bars track the location of the chambers in each wheel. They also measure the shape of each chamber over time. It does this tracking by using light sources placed on the chambers and viewed by the bars. This allows the alignment system to know the deformation of the chambers so that the measurements performed in the chamber can be transformed from the chamber's coordinate system to the global muon spectrometer system, and then to the global coordinate system for ATLAS. As discussed prior, the alignment system must do this measurement and transformation to an accuracy greater than $100\mu m$ before and after irradiation.[10]

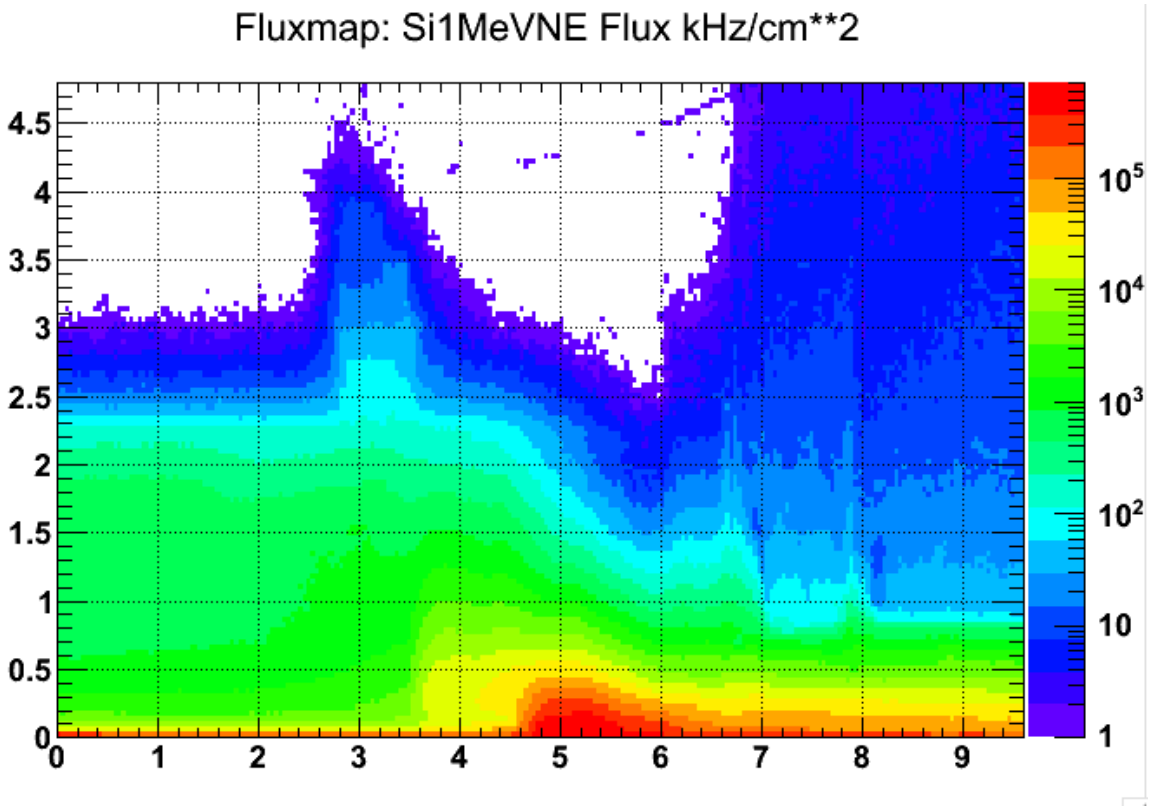

Figure 4: *This graph shows the simulated flux of* $1MeV$ *equivalent neutrons in Silicon in* $kHz * cm^{-2}$ *in ATLAS. The horizontal axis is the z-axis in ATLAS, or the distance along the beam line from the interaction point, and the vertical axis is the radius from the beam line. This assumes a beam energy of* $14TeV$ *but only a luminosity of* $10^{34}cm^{-2}s^{-1}$*.[9]*

3 Alignment Devices and Techniques

Brandeis High Energy Physics, or Brandeis HEP, has been critical in the creation of the alignment system for the muon spectrometer, and is currently working on the alignment system for the NSW. The current design for the NSW alignment system utilizes several different alignment techniques and Brandeis HEP has designed several new devices to perform the alignment. The main alignment techniques for the NSW are RASNIK mask imaging, light source imaging, and temperature measurements. All of these systems utilize devices created by Brandeis HEP that are either updated versions of ones currently being used in ATLAS or entirely new devices, and all of these devices and systems must operate in the increased luminosity environment.

3.1 Alignment Bar

The alignment bars are used to create the coordinate system in the NSW. They have an internal system that can measure the deformation of the bar, and an external system that creates the coordinate system. The internal system is composed of RASNIK mask imaging

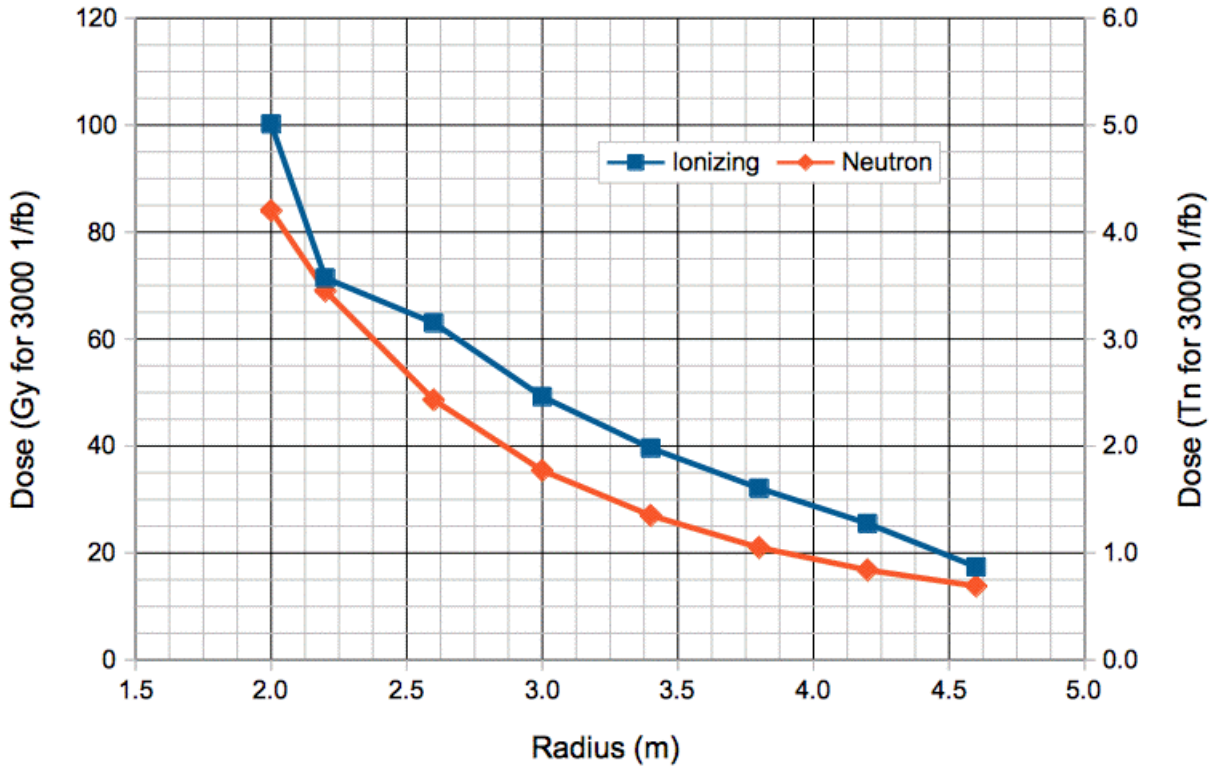

Figure 5: *Pictured is a plot of the simulated doses of ionizing radiation in Gray ($1Gy = 100Rad$) and neutron radiation in tera-neutrons ($1Tn = 10^{12}$ $1MeV$ Equivalent Neutrons/cm^2) after ten years in ATLAS with respect to distance from the beam line. This assumes a total integrated luminosity of $3000fb^{-1}$, which is the expected value after the upgrade, a beam energy of $14TeV$, and a z displacement of $7.5m$, which is where the NSW will be.[9]*

and temperature measuring systems, while the external bar system is composed of NBCAMs rigidly attached to the bar that view light sources. Both systems are controlled by our data acquisition software LWDAQ.[11]

3.1.1 Bar Head

The RASNIK mask imaging and temperature measurements are done primarily in the alignment bars. Inside the alignment bars are four RASNIK masks, four lenses, four CCDs, four RTDs (Resistance Temperature Detectors), and a bar head circuit board. The bar head circuit has a LWDAQ interface circuit, two CCD reading circuits that connect to two CCDs each via an extension board, four RTD resistance measuring circuits, and four LED array driving circuits. The RASNIK masks are back illuminated by an array of nine LEDs behind a diffuser, which are driven by the bar head. The RASNIK masks are viewed by CCDs read out by the bar head, through separate lenses inside the bar. Two masks are on a station on either end of the bar, and the CCDs are on two stations viewing the masks. The RTDs are placed on the CCD stations and the RASNIK mask stations, and connect to the bar head

circuit board by wires.[12] A drawing of an alignment bar for the NSW is shown in figure 6.

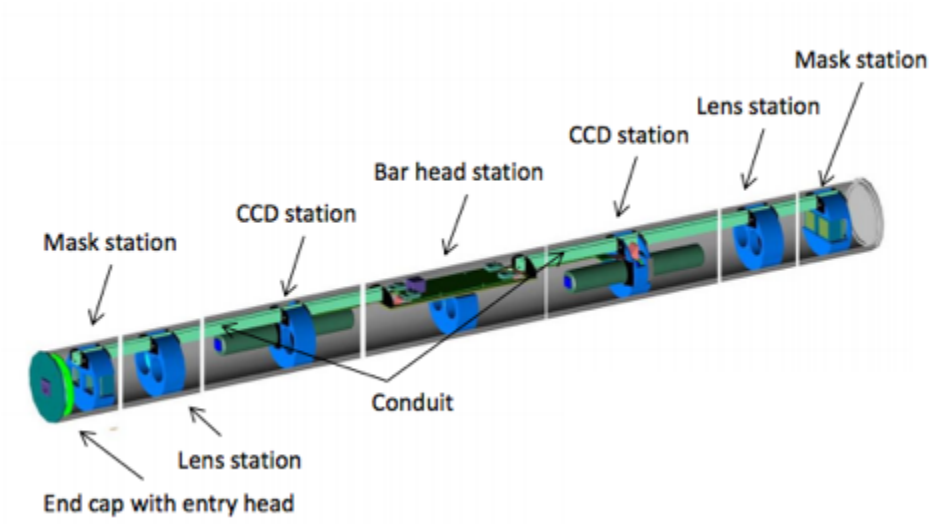

Figure 6: *Pictured is a drawing of an alignment bar for the NSW.[13] It has four RASNIK mask imaging lines and four RTD locations. Two of the RASNIK imaging lines are identical to the other two, just with a transversal displacement and then flipped.*

3.1.2 RASNIK Imaging

The RASNIK mask imaging can be done by using a CCD, a lens, and a RASNIK (Red Alignment System of NIKHEF) mask. The lens can be either a separate object or rigidly connected to the CCD creating a camera. The RASNIK mask has a black and white checkerboard pattern throughout the mask, except in every ninth row and column where the color of the square is flipped to encode a 1 or is left its original color to encode a 0. This allows a binary coding that gives the position of the 9x9 square in the mask. An image of a RASNIK pattern is shown in figure 7. For the alignment system of the NSW, the lens is used as a separate object to create a three point system of a CCD, a lens, and a RASNIK mask. The CCD uses the RASNIK encoding to determine the location it is viewing on the mask and then can track the deformation of the system as the camera's viewing location changes. If the lens were directly between the mask and the CCD, a $1\mu m$ transversal movement of the lens would appear as a $2\mu m$ movement of the mask on the CCD, which gives a move accurate measurement of displacement. Several 9x9 squares typically fit on the CCD, allowing redundant measurements of the position viewed on the mask. The image can also be analyzed to determine the rotation of the mask on the CCD.[10]

3.1.3 Temperature Measurements

The temperature measuring in the alignment of the NSW is done with RTDs (Resistance Temperature Detector). RTDs are small resistors with a known relation between the resistance of the RTD and the temperature of the RTD. By placing the RTD directly on an object that is large compared to the RTD, the temperature of that object can be measured

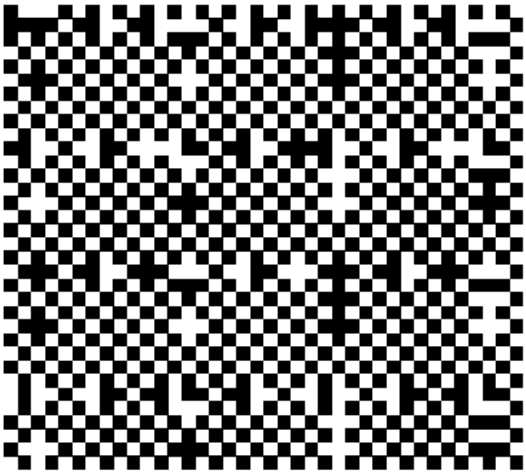

Figure 7: *Pictured is an image of a RASNIK pattern.[14] The flipping of the color in squares to break the checkerboard pattern encodes 1s and not flipping the color of squares encodes 0s creating a binary encoding. This is done every 9th row and 11th column for this RASNIK image, but for the NSW RASNIK masks this is done every 9th row and column.*

by measuring the resistance of the RTD attached to it. By using the temperature of an object and a relation for the expansion of that object with respect to temperature, we can estimate the expansion of the object as its temperature changes.[10]

3.1.4 NBCAM

The NBCAM (New Brandeis CCD Angular Monitors) is a CCD camera with a fixed lens, and is attached to the alignment bar. It uses a LWDAQ interface circuit, a CCD control circuit, a CCD mount connected to the circuit board via a flexible layer of the main circuit board, and a laser diode circuit board, which drives two separate laser diode circuits, connected by a flexible cable protruding from the main circuit board. The laser diodes are fixed to the faceplate of the NBCAM on either side of the lens. The laser diodes are calibrated to emit $1mW - 1.5mW$ of optical power. The lens is positioned so that an image is in exact focus when the object is $3m$ from the lens.[15]

3.2 Light Source Imaging

The light source imaging is done by NBCAMs in the NSW. The NBCAMs view either a laser diode rigidly connected to another NBCAM or a fiber optic source attached to a known location. The NBCAMs use a kinematic mount so their location with respect to what they are mounted on is known accurately. The NBCAM has a laser diode source on either side of its lens. A drawing of a NBCAM for the NSW is shown in figure 8. The separation of the

laser diodes is known and fiber optic sources are placed in pairs on the chambers with known separations, so when another NBCAM views the two sources one at a time, the distance from the NBCAM can be derived from the separation of the two sources as viewed by the CCD. Both laser sources and fiber optic sources can be used to measure transverse motion of the source with respect to the viewing NBCAM by monitoring how the position of the light source changes on the CCD over time and knowing the distance of the light source. Fiber optic light sources are placed on the chambers to track the chamber deformations, while the NBCAMs are on the alignment bars and view the fiber optic sources as well as create the coordinate grid in the wheel by viewing each other.[10]

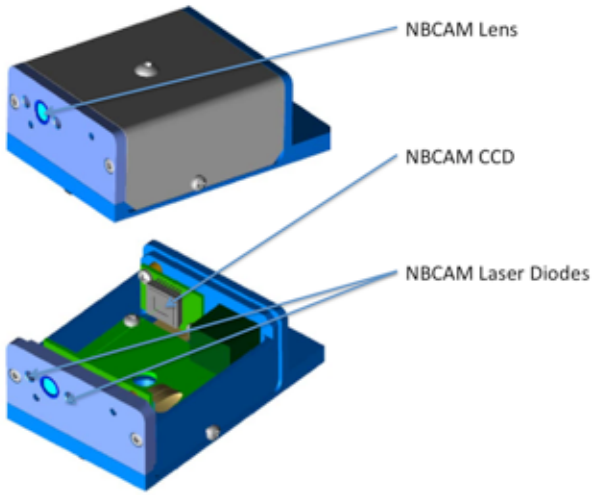

Figure 8: *Pictured is a drawing of a NBCAM for the NSW.[16] It shows the NBCAM's CCD, lens, and laser diode placements.*

3.2.1 Light Injector

The light source injection system is comprised of an injector that produces light for several sources, and fiber optic lines that have light injected into them at the injector and are run to the light source locations. The fibers then emit the light that is viewed by NBCAMs. The injector contains a LWDAQ interface (our data acquisition software) circuit and an array of LED (Light Emitting Diode) control circuits. The fiber optic cables have ferrules on either end to either emit or capture light. One end is placed directly against an LED in the injector to capture light, and the other end is the source for the NBCAMs to view. The injection circuit is currently designed to have an individual buck converter circuit for each LED, which takes in a DC voltage at a low current and outputs a lower DC voltage with a higher current to lower the power lost across cables, which have a resistance of $.1\Omega/m$.[17]

3.3 LWDAQ

All the systems examined and described in this paper are controlled and run by the data acquisition software LWDAQ (Long Wire Data AcQuisition). LWDAQ uses a driver to control LWDAQ devices via CAT-5 Ethernet patch cables. The driver is sent commands to be relayed to the devices. A Multiplexer is also often used in the alignment system, which takes one cable in from the driver and can have up to 14 separate devices connected to it. A repeater can be used between the Multiplexer and the driver to strengthen signals along long wires. The driver sends the command to the device through the Multiplexer by sending both the command to transmit to the device along with the socket number in the Multiplexer the device is attached so that the Multiplexer can relay that command to the correct device.[18] A diagram showing the different LWDAQ devices is shown in figure 9.

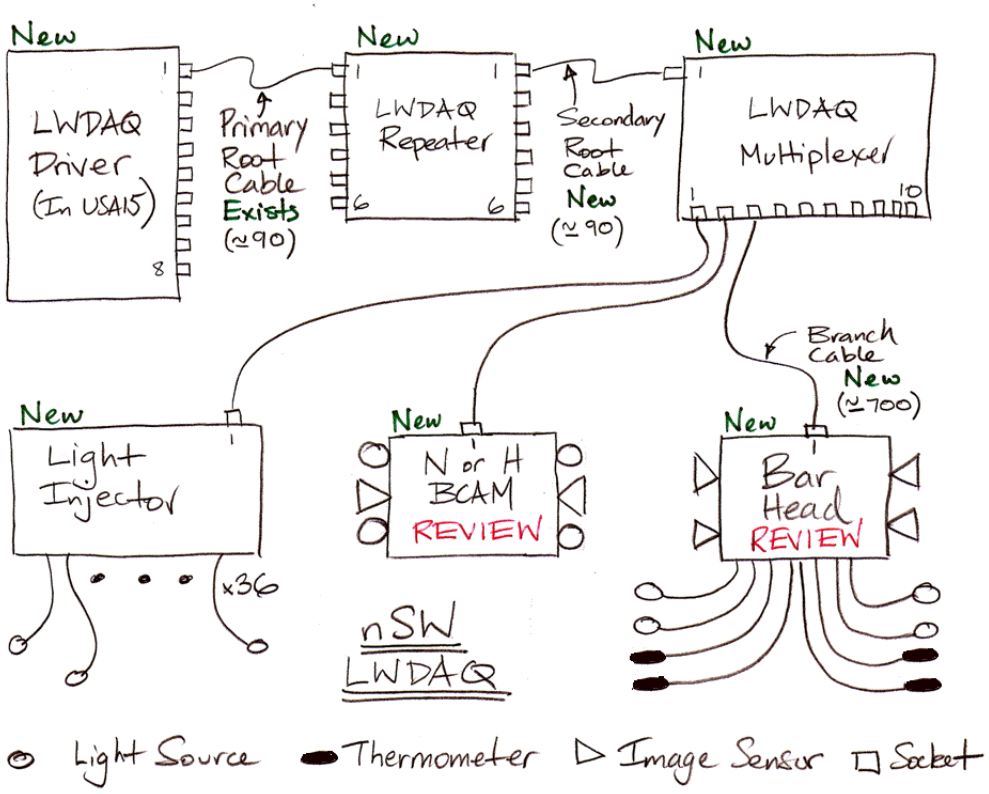

Figure 9: *Pictured is a drawing of different LWDAQ devices used in the NSW.[11] Devices labeled as new are ones being created or updated for the NSW. This is from a review report, so some devices are labeled as under review in this image.*

4 Ionizing Radiation Effects

Ionizing radiation is radiation of charged particles with energy great enough to free an electron from a molecule. If the particles have less energy than required, they will only excite electrons in the molecules; radiation of this type is considered non-ionizing radiation.

Phonons which travel through the material with energy of about $10eV - 33eV$ are typically the dividing line between ionizing and non-ionizing radiation. The phonons then cause the ionization of the atoms in the material.[19] The effects of ionizing radiation can be dose rate dependent, where the components affected by this type of radiation may anneal over time. Annealing is considered the apparent "healing" of a component over time after it has been damaged by ionizing or neutron radiation.[20]

The alignment system experiences ionizing radiation in the detector due to the debris from the high-energy proton-proton collisions. The amount of ionizing radiation a component experiences is primarily dependent on the distance that component is from the beam line.[9] In order to understand how the alignment system will operate in the detector overtime, the effect of ionizing radiation on the alignment system must be studied. Each component of the alignment system has been studied under varying levels of ionizing radiation.

The closest to the beam line any of the alignment system's components are is $2.2m$, at which they would receive about $70Gy$, or $7krad$, of ionizing radiation accumulated over ten years. This can be seen in figure 5 which shows the expected ionizing radiation doses over ten years in blue.[9] All components were studied at greater levels of ionizing radiation than is expected in the NSW. This was done in order to predict the safety factor of tolerance to radiation the system will have.

Electronic components can have varying effects from ionizing radiation. Almost all electronic components used were rad hard and unaffected by ionizing radiation up to $2kGy$. Most all components were well understood and tested in ionizing and neutron radiation for the original alignment system, and would function at the necessary levels for the circuits to operate correctly. Of the components that were not used in the original alignment system, most were fully functional after $1kGy$ of ionizing radiation. The components that are primarily affected by ionizing radiation are the P and N channel mosfets, fiber optic cables, and the ICX424AL CCD.[20]

4.1 Experimental Apparatus

Brandeis HEP has performed several different irradiation studies to determine the tolerances of our electronic and fiber optic components. We utilize two different photon sources for ionization experiments, as the photons can eject an electron by photoionization or Compton scattering, or it can pair production in the material. The freed electron or created electron/positron pair then cause ionization as well as photon radiation as the electron/positron bends in the material due to the Coulomb force. The radiated photons then can repeat this process, and so there is a shower of ionizing radiation as this process continues through the material.[21] Brandeis HEP has built a continuous x-ray source utilizing a $50keV$ x-ray tube. Brandeis has performed extensive studies to determine the dose rate in both air and silicon in Gy/hr at varying distances from the source. We also have utilized Brandeis's cesium-137 gamma source. The cesium-137 source emits $660keV$ photons which have an absorption coefficient that is almost exactly the same in air and silicon. Brandeis has also performed several experiments to determine the dose rate in Gy/hr for this source.[9] We have used both sources several times for our irradiation experiments, where we can accurately track the dose our circuits and fiber optic cables receive and can often track the change in behavior of these components as the dose increases.

4.2 P and N Channel Mosfets

P and N channel mosfets have three terminals: a source, a drain, and a gate. The two circuit representations are shown in figure 10. The mosfets can be used like a switch, where applying a certain voltage on the gate so that the difference between the gate voltage and the source voltage, called V_{GS}, passes a certain threshold turns on/off the mosfet. When on, current is able to flow through the drain and source terminals. For a P-channel mosfet, the voltage threshold to turn on the mosfet is negative, requiring a more negative V_{GS}, and current flows from the source to the drain. For a N-channel mosfet, the voltage threshold to turn on the mosfet is positive and the current flows from the drain to the source. When off, no current flows for either mosfet.[23]

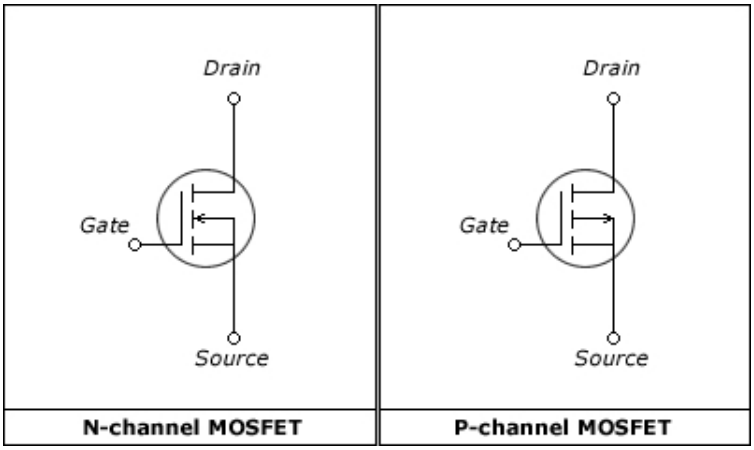

Figure 10: *Pictured is a N-channel mosfet and a P-channel mosfet circuit representation.[22] The arrow in the mosfet can be used to remember the direction current flows between the drain and source when the mosfet is on, since it always points in the opposite direction of the current.*

The P and N channel mosfets are used in the Bar Head circuit, the LWDAQ driver circuit, and the current design for the buck converter in the injection circuit. Brandeis HEP has performed extensive experiments on several P and N channel mosfets, with several different gate biases and levels of ionizing radiation, as well as under a gamma source and an X-ray source.[9] Utilizing our data, I was able to analyze the possible effects that the ionizing radiation would have on our circuits.

The Bar Head uses a NDS355AN mosfet, which is a N-channel mosfet, for each of its temperature measurement circuits. The NDS335AN has a gate voltage drop of $1.2V$ after $2kGy$ when a $0V$ bias is applied. The Bar Head was programmed to have a $0V$ bias on the mosfets when not in use, so almost all of the time the mosfet will experience a $0V$ bias. The NDS355AN has a typical gate threshold voltage of $1.6V \pm 0.5V$ as measured at Brandeis, and the maximum logic level 0 from the LC4128ZC is $0.1V$. From this, it is clear that the mosfets will still function at the necessary levels, since even after the $1.2V$ drop it will still have a threshold greater than the maximum logic level zero transmitted by the logic chip. The datasheet indicates the lowest threshold voltage of the NDS335AN can be $1.0V$ before damage, which would allow only a $0.9V$ drop, giving an ionizing radiation tolerance of $1kGy$.

With the mosfets seen at Brandeis so far, the tolerance is at least $2kGy$ due to the threshold voltage being $1.6V \pm 0.5V$. These results are no longer true if the gate bias is non-zero, where ionizing radiation causes greater damage to the NDS355AN.[9] When irradiated to $1.6kGy$, no other components of the Bar Head circuit, other than the CCDs, exhibited any faults or loss in functionality.[24]

The LWDAQ driver uses the NSD355AN N-channel mosfet, the NDS356AP P-channel mosfet, and the ZVN3306F N-channel mosfet. The driver will not be in the cavern with the rest of the electronics, but instead it will be in another room and therefore receive a much lower level of radiation. As described previously, the voltage threshold drop in the NDS355AN will not be enough to lose functionality of the mosfet as long as it has a $0V$ bias most of the time. The same is true for the driver, which will receive much less ionizing radiation. The NDS356AP mosfet has a voltage threshold of typically $-2V$, which drops to about $-3V$ after $2kGy$ of ionizing radiation with a $0V$ bias. This is a small enough drop that the circuit will function the same after this voltage threshold drop as it did before the voltage drop. The ZVN3306F's threshold drops from about $2.4V$ to $1.6V$ after $500Gy$ with $0V$ bias, to .9V after $500Gy$ with a $15V$ bias, and to $1.1V$ after $500Gy$ with a $-15V$ bias.[20] The driver is not planned to be in the radiation environment, and so it is much more tolerant to radiation than necessary.

The buck converter in the injection circuit uses the NDS356AP P-channel mosfet as a switch to allow current into the circuit from V_{in} or not. The circuit is shown in figure 11. The transistor at Q1 in the diagram is sent a $150kHz$ pulse with a duty cycle of about 7.5% that then causes the mosfet to turn on and off.[17] The voltage threshold dropping from $-2V$ to $-3V$ should not affect this operation to cause the buck converter to lose functionality.

4.3 Fiber Optic Cables

Fiber optic cables often darken after ionizing radiation, transmitting less light than it did originally. The optical fiber we have chosen to use is the S705T-02F-62N3 from Draka. Fiber optic cables have wavelength dependent transmissions, so we studied the cable at both varying levels of irradiation and different wavelengths. The Draka fiber has a $62.5\mu m$ radius core, which is the light accepting interior of the fiber, and a .275 numerical aperture.[25] A picture of the fiber cross-section is shown in figure 12. The fiber's transmission of light was primarily studied at $655nm$ and $456nm$ wavelengths, due to these being the wavelengths of the most promising LED sources. After $1500Gy$ a $2m$ fiber transmits 57% of the $655nm$ wavelength light and only 4% of the $460nm$ wavelength light. After this, primarily $655nm$ wavelength light was used for future studies because the shorter wavelength light would attenuate much more in the irradiated fiber. We have data on the transmission of $655nm$ light through a $1m$ fiber versus ionizing radiation shown in figure 13.[20]

The most irradiated fiber optic cable will be one that runs from the injector at $3.5m$ from the beam line to a source plate at $2.2m$ from the beam line. This fiber will be $2m$ long. The ionizing radiation levels are roughly linear with radius for these distances, seen in figure 5. I therefore averaged the radiation dose it would feel as $55Gy$. Our irradiation data is primarily with $1m$ fibers, but a $2m$ fiber can be considered as two $1m$ fibers, and so the transmission level of a $2m$ cable would be the square of the $1m$ transmission level. Utilizing the fiber radiation data, I was able to show that at $550Gy$, or an order of magnitude larger ionizing

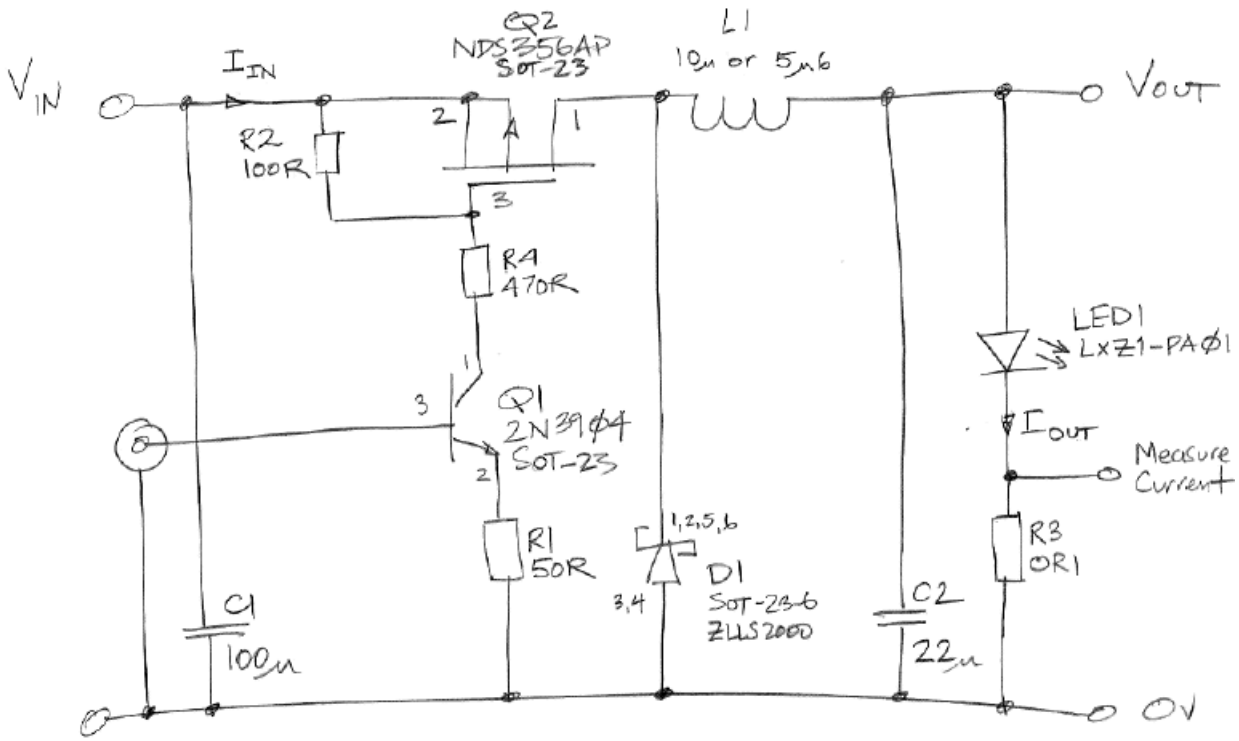

Figure 11: *Pictured is a diagram for a buck converter. This is the current design, but not the final design. Pin 3 of Q1 receives a pulse with a frequency of* $150kHz$*. R3 is used to measure current going through LED1 currently.[17]*

radiation than expected of the fibers, we would expect about 27.8% drop in transmission of $655nm$ wavelength light in a $2m$ fiber, which I then approximate to a 30% drop to be safe in my initial studies.[20]

4.4 CCD

The ICX424AL CCD can have dark current present when capturing images, and the amount of dark current is increased after ionizing radiation. Dark current is current measured in the CCD that is not created by photons freeing electrons when the CCD is capturing an image. Dark current is often caused by the crystal lattice in the CCD being damaged in some way, or electrons being absorbed into the insulators, which creates a static current source read by the CCD; the latter source of dark current is caused by ionizing radiation while the previous is how neutrons damage the CCD.[26] The dark current appears as light when taking an image, but can be partially accounted for by taking an image with the desired light source on and an image with it off, and then taking the difference between the two, which is called background subtraction. Dark current becomes a larger issue when it causes the CCD image to saturate. The CCD reads intensity of light in counts, where 200 counts correspond to about 0.5V generated from freed electrons with a 40-count pedestal, so a dark background is 40 counts.[15]

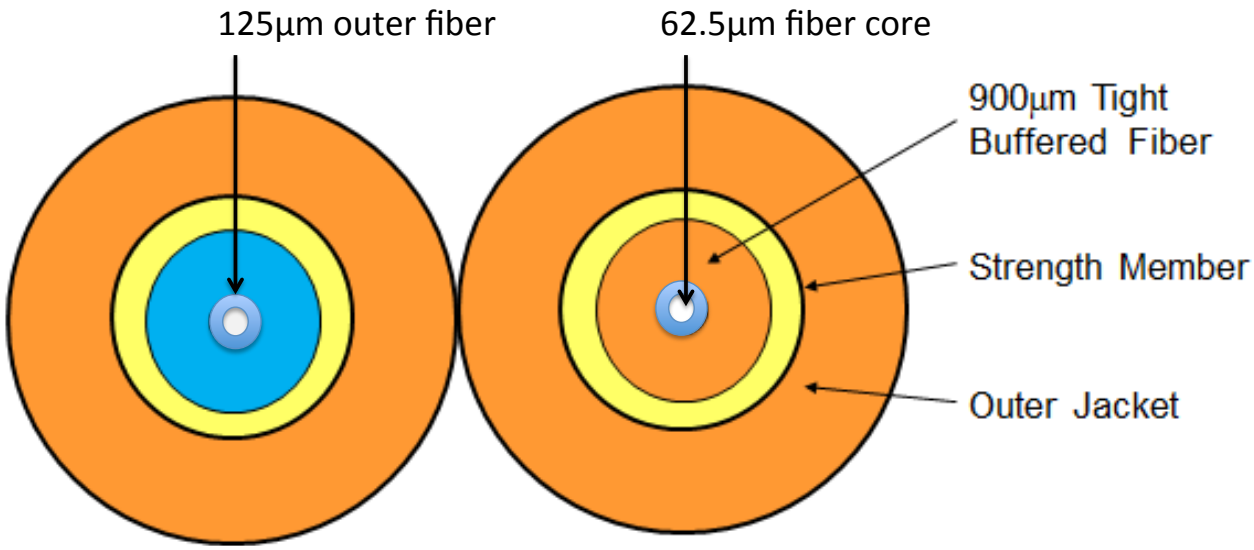

Figure 12: *Pictured is a cross-section of the S705T-02F-62N3 fiber optic cable from Draka. The two cross-sections are identical except for a jacketing color, which can be blue or orange. the innermost circle is the light accepting portion of the fiber, and has a numerical aperture of .275.[25]*

The CCD saturates at 255 counts, so dark current should not increase to the point where the exposure time for an image is enough time for the dark current to be close to saturating the rest of the image, preventing LWDAQ from telling apart the true light source and the dark current induced background. Dark current increases the intensity of the picture linearly with exposure time.[27][20] Brandeis has shown in the past that a spot creating a 20 count increase over the background is good enough to achieve the $400\mu m$ precision of the spot's location on the CCD, which is our required precision.[15] Dark current also increases the intensity while the image is in the transfer area of the CCD, where the CCD is transferring the data out row by row. The 504 rows in the CCD are read out one at a time, where the top row is read out first and the bottom row is read out last. Dark current linearly increases with ionizing radiation and at $475Gy$ the dark current is $.111counts/row$ when transferring the image out, and $15counts/ms/kGy$ from exposing for an image. This means that the background at $475Gy$ increases by .111counts every row of the image, down to the last row which is row 504, and that at a given dose g in kGy the background of the image increases by $15 * g$ counts for each ms of exposure time.[20]

5 Neutron Radiation Effects

Neutron radiation is when neutrons are emitted from a source and can interact with matter around them. Neutrons do not have any charge, so they can travel much farther than alpha or beta radiation particles.[28] The neutrons at the muon spectrometer have a

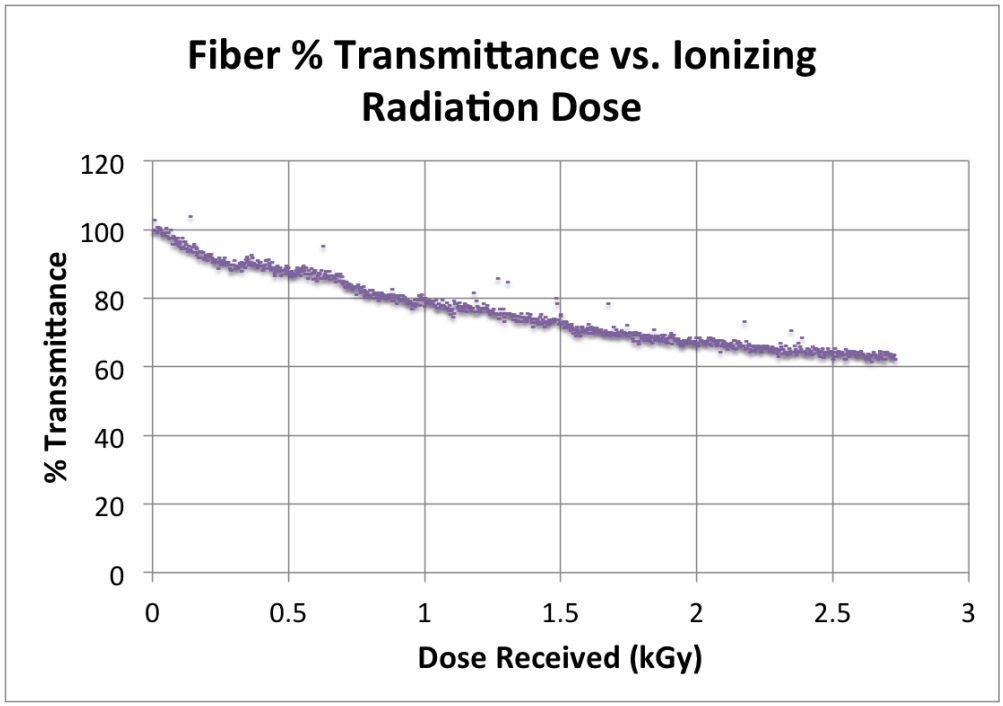

Figure 13: *Pictured is the measured transmission of* 655nm *light versus ionizing radiation for the Draka fiber.[20]* 456nm *light was not used in this experiment due to already being shown that it attenuates much more than the* 655nm *light.*

high energy, on the order of a MeV, and they can displace a silicon atom in the crystal lattice of a CCD creating a current source for the CCD,[26] or cause local melting where they impact.[29]

The alignment system experiences neutron radiation in the NSW, where the dose is dependent on the distance from the beam line as shown in figure 5.[9] Different components of the system respond differently to neutron radiation, and components that were unaffected by ionizing radiation may be vulnerable to neutron radiation, and vice versa. The main components affected by neutron radiation are the ICX424AL CCD and the Luxeon-Z LEDs.[27]

5.1 Experimental Apparatus

Brandeis does not have a neutron irradiation apparatus, so we utilize the neutron irradiation apparatus at University of Massachusetts Lowell. They offer the ability to irradiate our components with high energy neutrons and calculate the dose they received.[27] The radiation damage we receive does not depend on how quickly the damage happens, but instead on the total energy delivered from the neutrons. Due to this, we can measure neutron radiation by the number of $1MeV$ neutrons that would equate to the radiation the material received. We therefore discuss neutron damage in terms of $1MeV$ equivalent neutrons. We also define a useful unit called "Tn," or tera-neutrons, which stands for 10^{12} $1MeV$ equivalent neutrons/cm^2.[9]

5.2 CCD

The ICX424AL CCD also has an increase in dark current after neutron radiation. A CCD utilizes silicon to create a near perfect crystal lattice. The neutrons damage the crystal lattice in the CCD and often cause a pair production that becomes a static current source read by the CCD. The closest to the beam line it is in the NSW is $2.2m$, which corresponds to about $3.5Tn$. The dark current in the CCD increases linearly with neutron radiation, at about $.115counts/(ms * Tn)$ when capturing an image for a given amount of milliseconds, and $.058counts/(ms * Tn)$ when transferring the image from the CCD. It takes $180ms$ to transfer a full image, so the transfer damage can be considered as $10.44counts/Tn$.[27]

5.3 Luxeon-Z LED

The Luxeon-Z LEDs are currently the LEDs we will use for the light source in the injector and the light source to illuminate the RASNIK masks. We have the Deep Red Luxeon-Z LED with a wavelength of $655nm$ and we have the Royal Blue Luxeon-Z LED with a wavelength of $456nm$. The Royal Blue LEDs drop only 20% of their power after $16Tn$ of neutron radiation. The Deep Red LEDs are expected to receive about $1.2Tn$ of neutron radiation. After $16Tn$ of neutron radiation, the optical power of the Deep Red LEDs drops by 74.7%. Due to the radiation hardness of the Royal Blue LEDs, they will be used in the RASNIK mask illumination. The Deep Red will be used for the light injection though since blue light attenuates in our fibers much more after ionizing irradiation.[27]

6 Tolerance Estimations

The alignment system must be able to tolerate the expected dose of neutron and ionizing radiation, and our goal is to have a safety factor of 5. Utilizing the radiation effects on the NSW components, I was able to estimate the tolerance our system has to neutron radiation and ionizing radiation. I analyzed the data and information we had for the RASNIK mask imaging, fiber source imaging, and laser diode source imaging. The maximum dose of ionizing radiation any circuit will receive in the NSW is $70Gy$. The circuits containing NDS355AN and/or NDS356AP mosfets can at maximum receive a dose of $2kGy$.

The radiation tolerance of the CCD is the amount of neutron and ionizing radiation it can tolerate before it can no longer take an image of a light source with a high enough count intensity above the background intensity without saturating. The count intensity needed above the background is given from the need of $400nm$ resolution on the NBCAM CCD, where resolution versus spot intensity is shown in figure 14. This corresponds to about a need for at least a 30 count spot, but the resolution can be improved for the lower count spots by taking the image multiple times so that a 10 count spot can still satisfy the correct resolution.[15] For now, I assume the spot needs to be at least 30 counts. To determine this amount of radiation, I needed to know the exposure time it would take for a good image with the RASNIK mask lines, the fiber optic sources, and the laser diode sources before and after radiation. These each have both different light sources as well as varying distances, so I derived each of them separately.

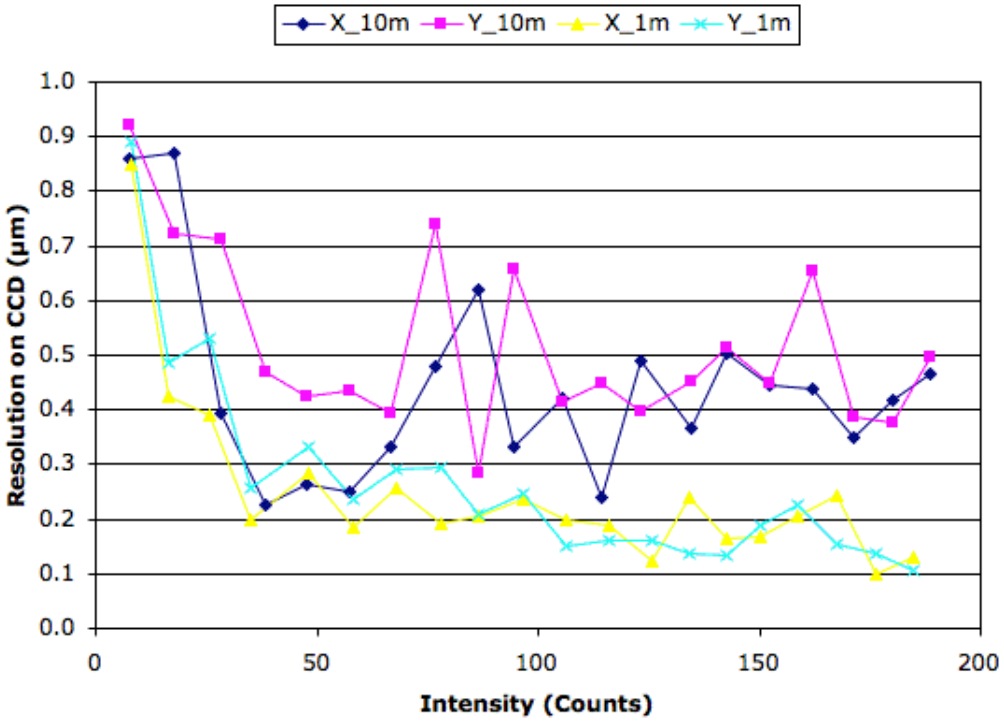

Figure 14: *Pictured is a plot of BCAM resolution versus spot intensity for two different source distances of* $1m$ *and* $10m$*.[15] The largest range in the NSW is* $3m$ *which has a resolution similar to the* $1m$ *range.*

6.1 Fiber Source Exposure Time Estimations

The fiber source imaging is performed by a NBCAM taking an image of light produced by a Luxeon-Z Deep Red LED and transmitted by a fiber optic cable. Through several experiments, I was able to show that the Luxeon-Z LEDs can be driven at $1Amp$ continuously with proper heat sinking without becoming damaged. I also showed that with a duty cycle of 10%, a frequency of $10Hz$, and proper heat sinking, the LEDs can be driven up to $4Amps$. Our goal is to avoid implementing a system that cannot have a light accidentally left on, since this would require more complex circuitry, firmware, and/or software, so I considered $1Amp$ to be a temporary maximum current. I found that the Deep Red LED emits an optical power that is approximately proportional to its current, with a ratio of power to current being about .8. At $1Amp$, the Deep Red LED emits about $840mW$ of optical power on average. The data sheet gave a graph of the LED's angular intensity, so I created an approximation to the angular intensity to use for future calculations. I did this for the Royal Blue LED as well. Using the area of the LED, the area of the fiber core, the approximation of the Deep Red LED's angular intensity, as well as the numerical aperture of the fiber, I was able to show that only .01% of the produced light from the LED would be captured by the Draka fiber.

Using the .01% of the light being captured by the fiber and the assumption that the emitted light would have the same angular intensity as the captured light, I used the size of the lens of the NBCAM to predict the amount of light emitted by the fiber that makes it

to the lens at varying distances. This general setup is shown in figure 15. I then assume for most distances the spot is approximately in focus, so that the image appearing on the CCD is a Gaussian distribution of light, where the Gaussian is only a function of wavelength, the lens diameter, and the distance the lens is from the CCD. The spreading of the light intensity is plotted in figure 16. The amount of light reaching the lens of the NBCAM, assuming it is farther than $10mm$ where the numerical aperture of the fiber affects the solution, can be expressed as:

$$(\int_0^{ArcTan(.001/R)} I(\theta)d\theta / \int_0^{\pi/2} I(\theta)d\theta) * (A_{fiber}/A_{LED})$$

where $I(\theta)$ is the angular intensity function of the LED, A_{fiber} is the area of light capturing fiber core, A_{LED} is the area of the light emitting portion of the LED, R is the distance the fiber tip is from the NBCAM lens, and ArcTan(.001/R) can be approximated as .001/R for all relevant distances in the NSW. The numerical aperture can be ignored since the fiber acts as a wave guide, so the angular intensity of the light is unchanged, and the lens is far enough away such that the center cone of light is independent of the size of the cone of light emitted by the fiber.

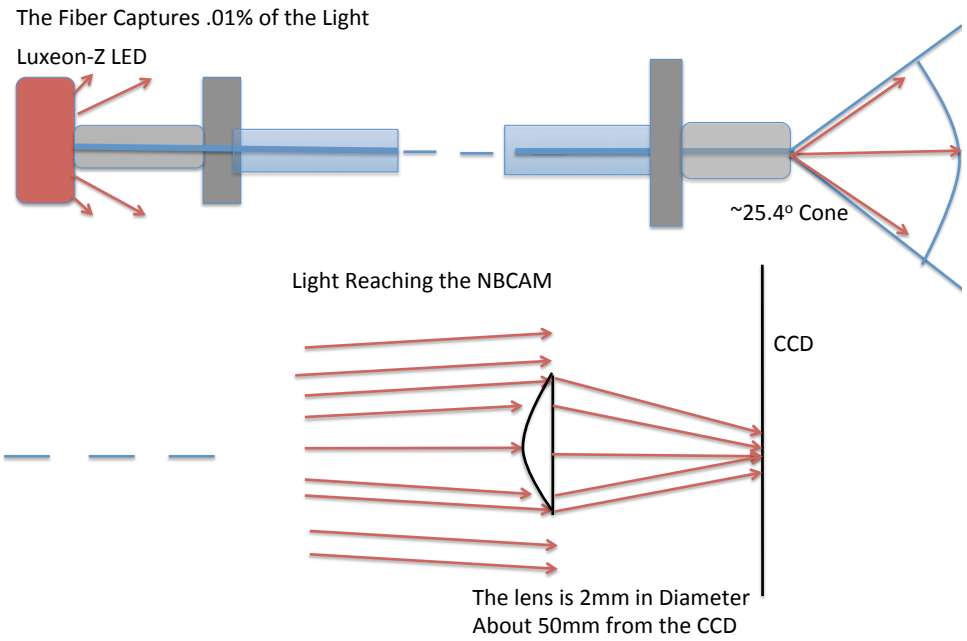

Figure 15: *Pictured is the general setup of fiber optic imaging. It shows a fiber optic cable capturing light from an LED, and then emitting the light from the other end of the cable. The lens then captures and focuses a portion of that light onto the CCD.*

I defined a good spot for detection purposes to be one whose peak intensity was between 170 and 190 counts on the CCD, where peak intensity is the largest intensity pixel in that spot. This is including the 40 count pedestal, and would be without considering dark current which increases the background. As dark current increases the intensity of the background,

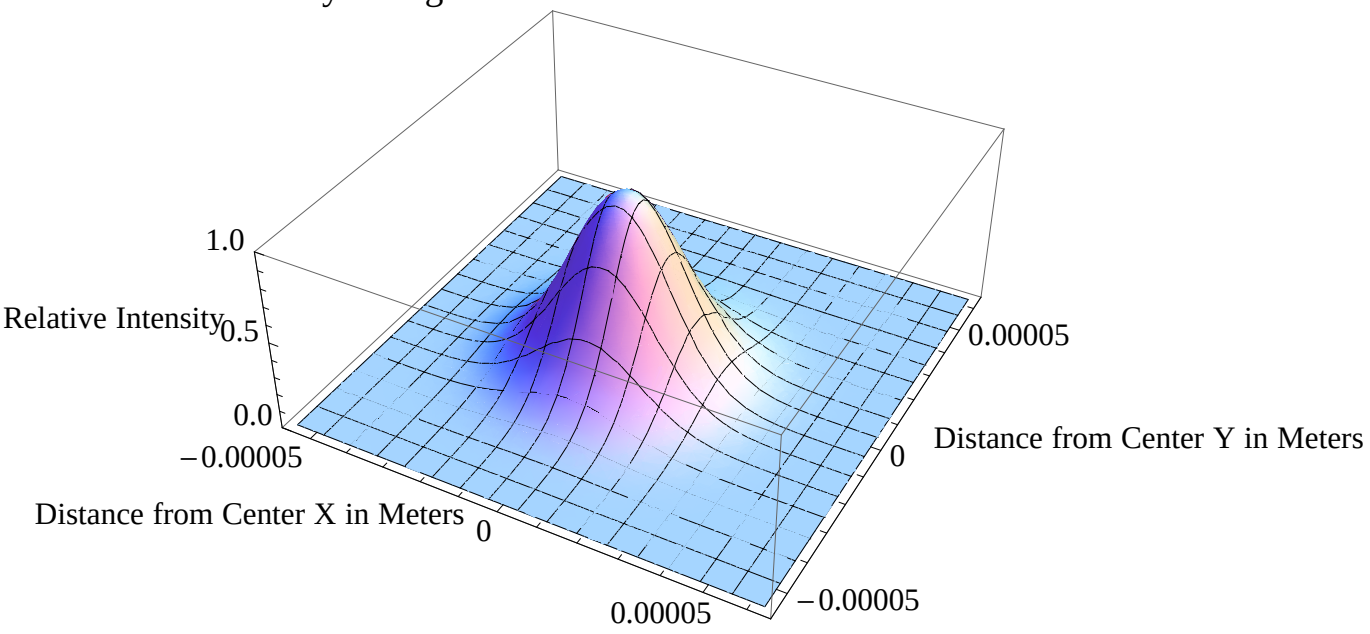

Figure 16: *Pictured is the relative intensity of light on the CCD for* $655nm$ *light and a* $2mm$ *diameter lens positioned* $48mm$ *from the CCD versus the distance from the center of the spot in meters. This plot assumes a perfect focus, which occurs at* $3m$ *from the NBCAM. Each square in the grid is roughly the size of the pixel on the ICX424AL. which is a* $7.4\mu m$ *square. This shows how the intensity of the light is only spread among a few pixels of the CCD, where 24% of the light is in the first pixel alone.*

the peak intensity can be lowered to a minimum of 30 counts above the background. 170-190 counts was initially picked as the range for a good spot as this was the value chosen for the old CCD which would have spot distortions as pixels began to saturate, but this problem does not happen for the ICX424AL.

To estimate the peak intensity of the incoming light, I found the number of photons per second that would be in the center of the Gaussian within the area of a pixel. I used the LED's data sheet's distribution of power with respect to wavelength to find the number of photons emitted by the LED, and then showed that this was equivalent to assuming a single wavelength of $655nm$. The two different approaches I showed were equivalent were:

$$\int_0^\infty (P_o * P(\lambda) * \lambda/c/h)d\lambda = P_o * \lambda_o/c/h \implies \int_0^\infty P(\lambda) * \lambda d\lambda = \lambda_o$$

where P_o is the power of the LED in Watts, λ_o is the given wavelength of the LED, c is the speed of light, h is Planck's constant, and $P(\lambda)$ is the normalized distribution of power with respect to wavelength of light emitted. This simply shows that the dominant wavelength given is equivalent to integrating along the wavelength distribution function, which is shown in figure 17. The wavelength distribution also has a very small width, so that the light can be considered a single wavelength when considering the CCD's wavelength dependent response.

To estimate the intensity read by the CCD, I would need the quantum efficiency of the CCD, which is the ratio of the number of electrons freed to the number of photons of a

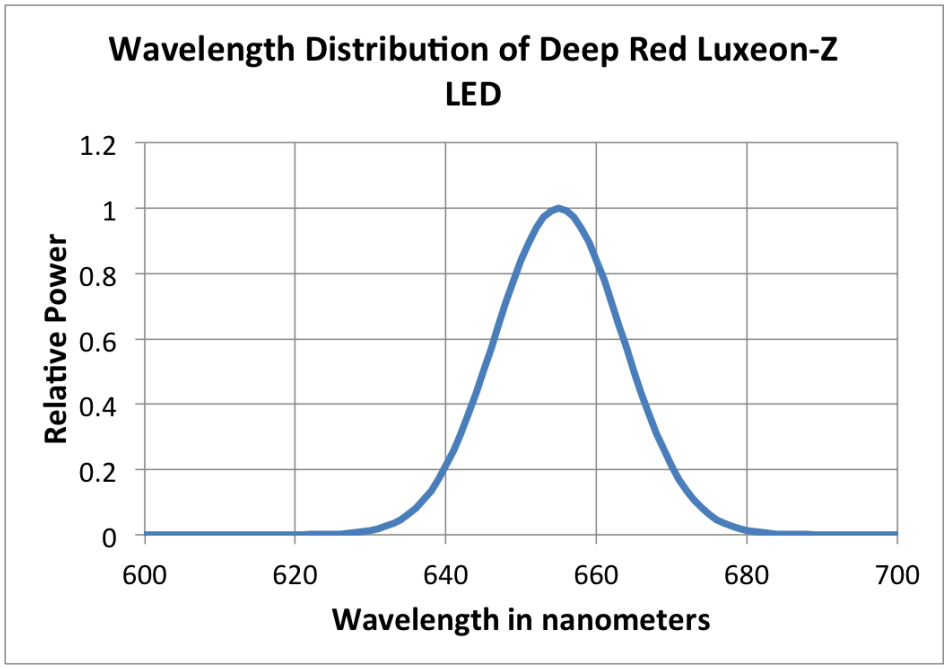

Figure 17: *Pictured is the relative power of the Deep Red Luxeon-Z LED with respect to wavelength. $P(\lambda)$ is the relative function normalized.*

certain wavelength it took to free them, and the charge conversion of the CCD, which is the electric potential increase due to each freed electron. The CCD uses the electric potential increase in a pixel to measure the intensity of light viewed by it. These values were not given to us with the CCD, but I estimated them based on the quantum efficiency of two cameras I found utilizing the ICX424AL. A graph of these cameras quantum efficiencies are shown in figure 18. The quantum efficiency is .3 for $655nm$ light for these cameras,[30] so I used values near this for my estimates, along with a typical range of charge conversion values, $5\mu V/electron$ to $10\mu V/electron$.[31] I also used the fact that half a volt from freed electrons was equivalent to about 200 counts including the pedestal on the CCD with our current circuit, and that counts increased linearly with electric potential. Utilizing this information, I estimated a range of possible exposure times at different distances from the source, as shown in figure 19. The equation used was:

$$t = mV/(cc * QE(\lambda) * fp * Ph(R))$$

where t is the exposure time in milliseconds, mV is the millivolt potential desired on the CCD, cc is the charge conversion of the CCD in Volts per electron, QE(λ) is the quantum efficiency of the CCD at a wavelength λ, fp is the percent of the photons that reach the center pixel, and Ph(R) is the number of photons reaching the CCD per second at a distance R from the source.

6.2 Laser Diode Exposure Time Estimations

I utilized the laser diode's datasheet and its calibrated power to estimate exposure times for NBCAMs viewing other NBCAMs. During this estimation, I gave a more narrow range

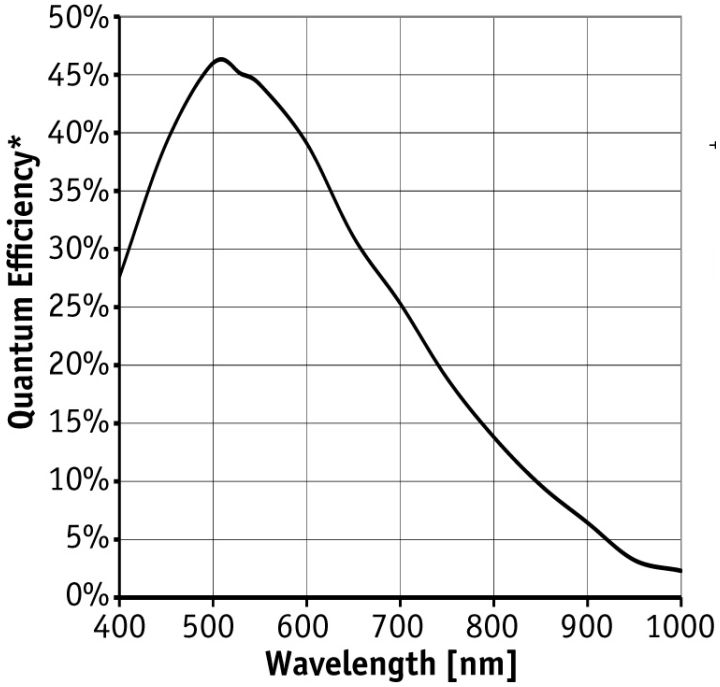

Figure 18: *Pictured is the quantum efficiency given for two cameras utilizing the ICX424AL with respect to wavelength. The asterisk on the y-axis title denotes that the quantum efficiency plotted is without adding protective glass or filters to the CCD.[30] I removed the plot of the quantum efficiencies for different filters from this image.*

of CCD peak intensity values, choosing it to be between 180 and 190 counts. The laser diodes also have a wavelength of $655nm$. The laser diode has a much more narrow angular intensity function, which is described by two orthogonal Gaussians.[32] I approximated this as a single Gaussian with a width equal to the average radius of an ellipse with semi and major axes equal to the two Gaussian widths. Since there is no fiber capturing the diode's light, I used the approximation to the angular intensity and the measured power to directly determine the amount of light making it to the NBCAM's lens. I then used the same Gaussian distribution of light on the CCD as with the fiber source, once again assuming a perfect focus, to determine the amount of light reaching the center pixel. I used the same range of quantum efficiency and charge conversion values as with the fiber source. The plot of the range of possible exposure times versus distance from the source is shown in figure 20.

6.3 Radiation's Effect On Exposure Time

To include the effect of irradiation, I then plotted the possible exposure times as total transmission of light dropped in the system. For the laser diode viewing, there is no effect from irradiation except the increase in dark current in the CCD. For the fiber source viewing, the LED's power drops by 74.7% after $16Tn$ and the fiber optic cable's transmission drops by about 30% after $550Gy$ for the longest lines. This means that the total light received

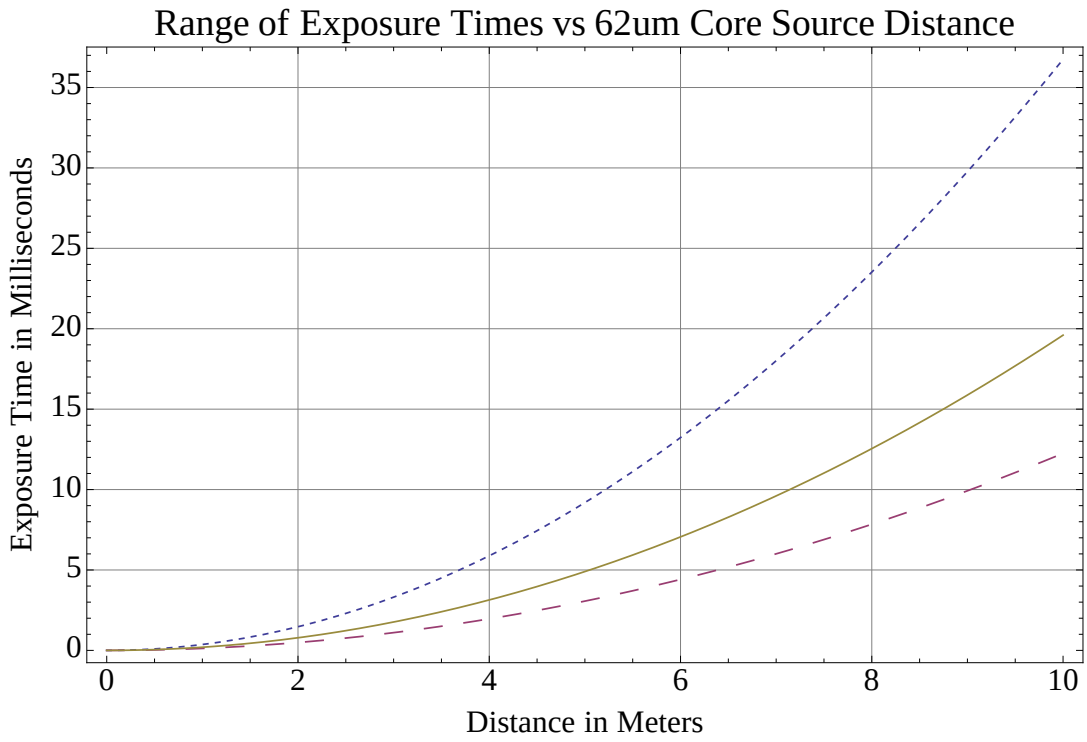

Figure 19: *Pictured is an estimated range of exposure time times versus distance when viewing the fiber optic light source, where the blue line with small dashing uses a charge conversion of* $5\mu V/electron$ *and quantum efficiency of .2, the yellow line without dashing uses a charge conversion of* $7.5\mu V/electron$ *and a charge conversion of .25, and the pink line with large dashing uses a charge conversion of* $10\mu V/electron$ *and a quantum efficiency of .3.*

by the CCD will drop to 17.7% of the light it would receive without $16Tn$ and $550Gy$ of irradiation. I plotted the exposure time on the CCD with several quantum efficiency and charge conversion values as transmission drops from 100% to 17.7%. I used a more narrow range of distances, going only up to $3m$ since this is the maximum distance from a fiber source a NBCAM will be. The plot of exposure time versus both transmission and distance from the source is shown in figure 21.

6.4 RASNIK Mask Exposure Time Estimations

I measured the power emitted from a RASNIK mask illuminated by Royal Blue Luxeon-Z LEDs, to predict the exposure times on the CCD. I utilized the optical power emitted across the mask along with the lens's focal length, the mask positions, the lens positions, and the CCD positions to derive the exposure times for each of the four lines inside of the alignment bars. Due to the symmetry in the RASNIK mask lines, there are only two unique lines. I used the area of the CCD and mask along with the magnification of the mask by the lens to predict the exposure times with varying quantum efficiencies and charge conversions. I assumed that the white squares in the RASNIK image were all equally as bright, and so the peak intensity would be the same in all of the white squares. The quantum efficiency

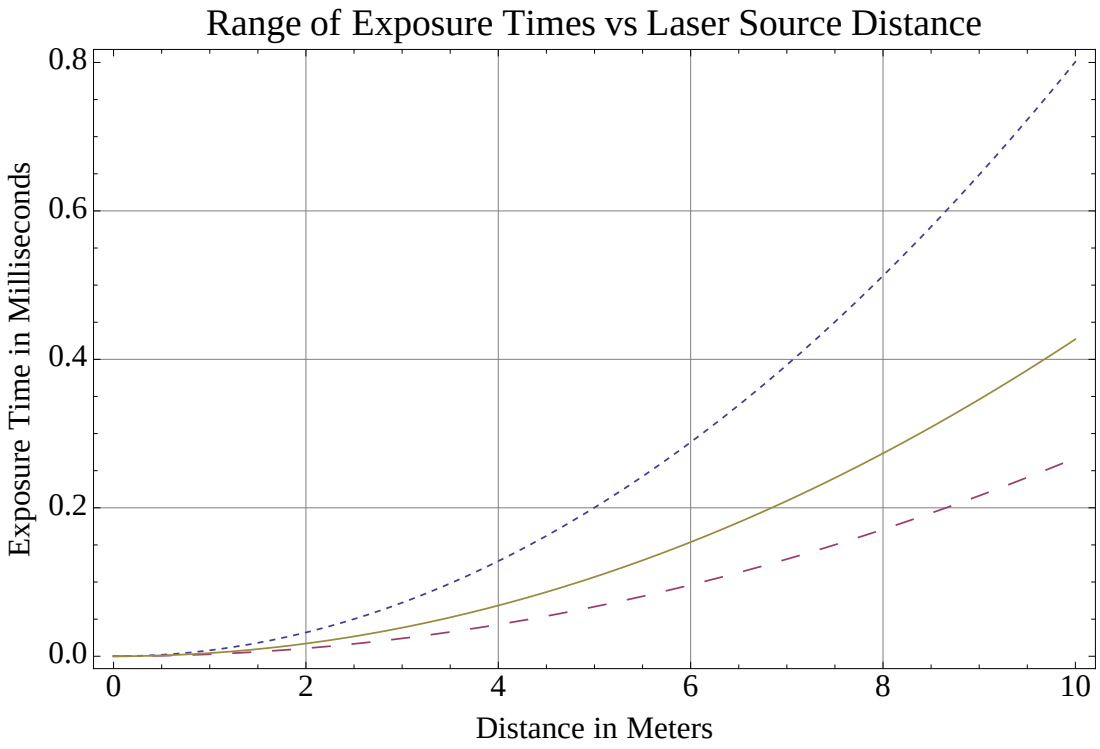

Figure 20: *Pictured is the range of possible exposure times versus distance with different charge conversions and quantum efficiencies for viewing the laser diode. The blue line with small dashing, the yellow line no dashing, and the pink line with large dashing represent the same charge conversion and quantum efficiency values as they did in figure 19.*

I varied around was .39 due to that being the quantum efficiency of two cameras I found, which both use the ICX424AL.[30]

The dark current in the ICX424AL increases with exposure time, as discussed before. Utilizing the estimated exposure times on the CCD, we can predict the tolerance of the image viewing system to radiation. As the dark current increases, we can scale down the exposure times to be less intensity on the CCD while still greater than 30 counts above the background. The tolerance of the system would then be the maximum amount of ionizing radiation and neutron radiation that the system can tolerate before the CCD cannot capture a spot with at least 30 counts above the background without having the dark current saturate the image. To determine this tolerance, the charge conversion and the quantum efficiency must be determined so we can more accurately predict the exposure times on the CCD at varying distances and intensities above the background.

7 Experimental Measurements

In order to better understand the tolerance of the alignment system to radiation, I performed several experiments on different components of the system. The main experiments I performed were exposure time experiments on the ICX424AL with different light sources

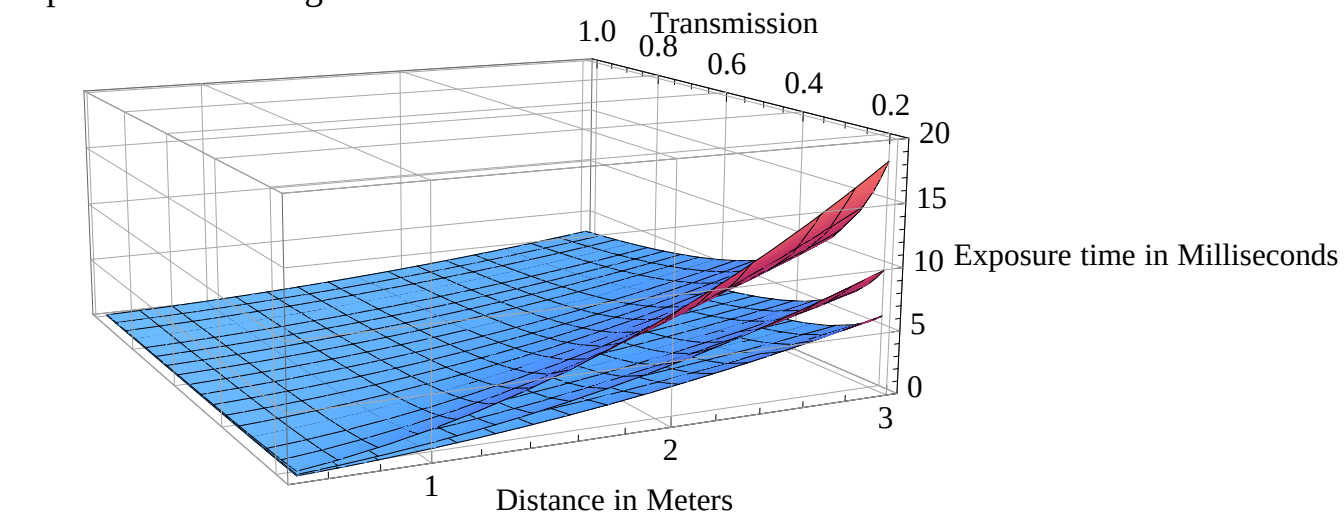

Figure 21: *Pictured is the range of exposure times versus distance from source and the transmission coefficient due to irradiation. The top sheet, middle sheet, and bottom sheet have charge conversion and quantum efficiency values that correspond to the blue line with small dashing, the yellow line without dashing, and the red line with large dashing in figure 19 respectively.*

and fiber optic cables, as well as power measurements for several different light sources. My goal was to obtain the maximum amount of light we can deliver safely in the different parts of the system as well as experimentally derive unknown values such as the charge conversion of the ICX424AL.

7.1 Power Measurements

I first measured the power from a Luxeon-Z Deep Red LED when mounted on a circuit board I designed as well as a heat sink I made bolted to the circuit board. Utilizing this set up, I was able to drive the LED continuously at $1Amp$ and could pulse it at a 10% duty cycle with a period of 100ms up to $4Amps$. At $4Amps$, the LED would begin to heat so rapidly that it would drop in power within the 10ms it was on for. For any current above $1Amp$ the LED's temperature would rise above $130°C$, which we set as the maximum allowed temperature, though the data sheet suggests the LED is fine up to $150°C$.[33] I then left the LED on at $1Amp$ continuous current for a couple days to ensure it would not break or lose optical power at that current, and there was no noticeable loss in functionality after being left on.

I then tested the ADL-65055TL laser diode that is used in the NBCAM. I measured the laser's power with respect to current and found that power was linearly dependent on the current supplied. I calibrated the laser board circuit by varying a current controlling resistor so that the laser diodes would output $1.5mW \pm .25mW$ when driven by the NBCAM. I then flashed the laser diode a few million times to ensure that it would survive the 10 years in the NSW at this current. It was undamaged after the several million flashes, and the data

sheet specifies that it can be run up to $5mW$ without damage.[32]

The Deep Red LED's light is injected into a fiber optic cable for the system, so I measured the power captured by both the Draka $62.5\mu m$ core fiber with numerical aperture .275[25] and a CeramOptec WF100/110P37 $100\mu m$ core fiber with numerical aperture .37.[34] For varying LED currents, the resulting power is within 10% of my predicted power emitted by the fibers. This shows that my formula for calculating the percent of light captured by the fiber as a function of the LED's angular intensity, the fiber's numerical aperture, the LED's area, and the fiber core area is accurate to at least 10%.

7.2 Exposure Time Measurements

Using the Luxeon-Z circuit I designed with its heat sink, a programmable circuit board, a mosfet controlled by the programmable circuit board, and a power supply, I was able to make a prototype injector that injects light from a Deep Red LED driven at $1Amp$ into a fiber optic cable and is controlled by LWDAQ for accurate flash times. This prototype injector was also capable of driving Royal Blue Luxeon-Z LEDs, but I did not test the injector with them due to $456nm$ light attenuating in irradiated fiber optic cables.[20] Using this prototype injector, I measured the exposure times for a BCAM to reach between 170 and 190 counts when viewing the Deep Red LED's light injected into the Draka $62.5\mu m$ core fiber from a range of $.5m$ to $10m$. I performed these measurements using a flat optical rail. I then measured the exposure times for the same BCAM and the same injector set up but with a $100\mu m$ fiber. I found that the ratio of the two times was a function of the ratio of the two fibers areas and not the numerical aperture, as expected since the light that matters is the light in the forward direction and not the entire cone of emitted light. The plot of the exposure times on the BCAM when injecting light with two different core diameter fibers is shown in figure 22.

I used an NBCAM to repeat the above experiment with the Draka $62.5\mu m$ core fiber, to compare the exposure times of the old BCAM to the NBCAM. I also repeated the experiment again using the Q setting on the NBCAM's ICX424AL, which binds pixels together to form pixels with four times the area.[24] The relevant portion of these experiments is the range from .5m to 3m, as this is the range of distances seen in the NSW. Using these, I showed that before irradiation we are able to image a spot between 170 and 190 counts at 3m in 1.1ms with the NBCAM taking images normally and in about .5ms utilizing the Q setting. The old BCAM needed about 2ms to capture the same spot at the same peak intensity. The plot of these exposure times is shown in figure 23.

After ionizing radiation experiments were performed on the ICX424AL, Brandeis HEP found that the CCD was gaining too much dark current at lower ionizing radiation levels than excepted. We found that by lowering the clock voltages, we were able to reduce the effect ionizing radiation had on the CCD in the form of dark current, as the background increased less with these new clock voltages. CCDs that had already been damaged by ionizing radiation also performed better with the new clock levels, so it was not that the lower clock voltage necessarily prevented damage but instead was reducing its effect. The radiation results I have presented have been assuming this change in the circuit. This change caused the ICX424AL Q setting to offer no advantages against radiation though, having no less dark current after ionizing radiation than without the Q setting. We therefore decided

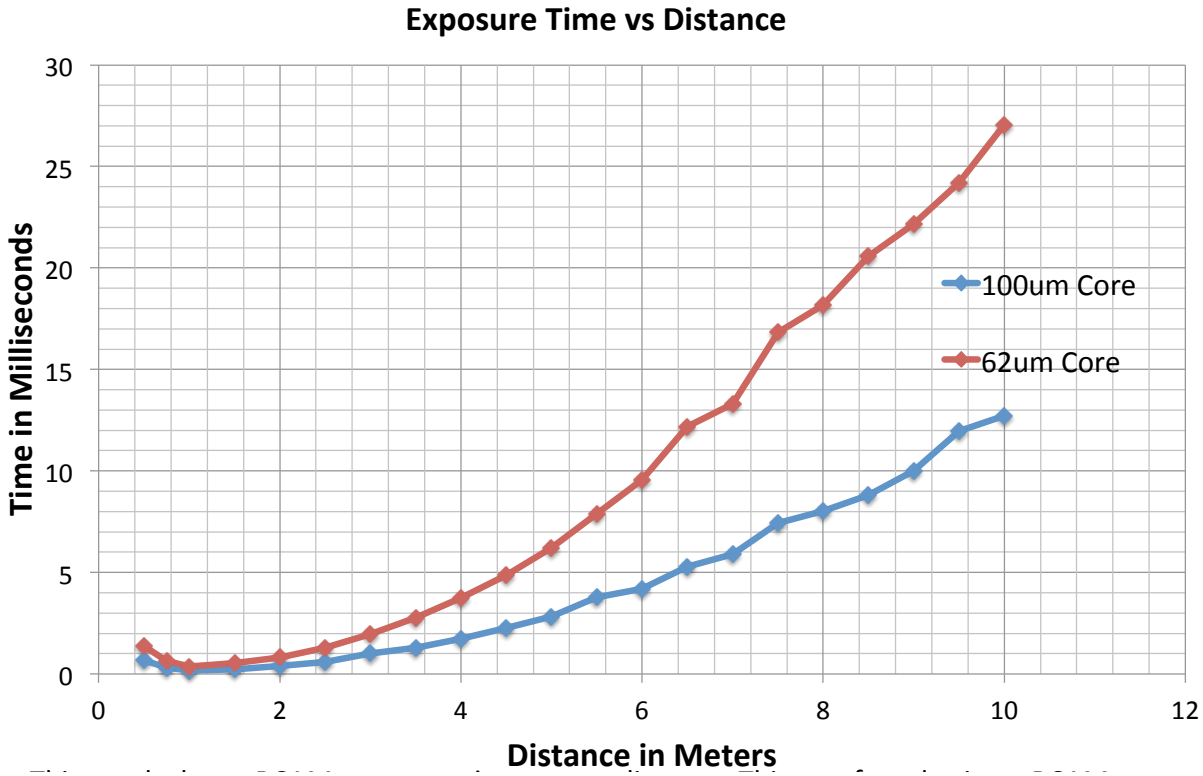

Figure 22: *Pictured are the measured exposure times of a BCAM viewing light from a Deep Red Luxeon-Z LED driven at* $1Amp$ *injected into a* $62.5\mu m$ *core fiber and a* $100\mu m$ *core fiber at varying distances. Exposure time was measured as the amount of time to achieve a spot with peak intensity of 170-190 counts.*

to not use this setting in the NSW, and so I no longer performed experiments utilizing it.[20]

To measure the laser diode exposure times, I set up an NBCAM in place of the injector on the optical rail. Using another NBCAM, I measured the exposure time on the ICX424AL needed to get a spot with peak intensity between 180-190 counts. I used a more narrow range so that different data points would be more likely to have the same peak intensity. I measured the exposure times from .5m to 10m. I did not perform the same measurements using the Q setting on the ICX424AL due to using the setting after irradiation offering no radiation tolerance improvements having been discovered by this point in time. The plot of measured exposure times is shown in figure 24.

7.3 Theoretical and Experimental Comparisons

I plotted the laser diode source data on the same graph as the exposure time estimates I had made with varying parameters. I assumed a quantum efficiency of .3 due to the cameras I had seen using the ICX424AL having that quantum efficiency,[30] and found that the charge conversion for the data should be about $7.68\mu V/electron$ by using a fitting function. Figure 25 shows the measured data on the same plot as the estimated range of exposure times, and figure 26 shows the estimated exposure times with the fitted charge conversion value with

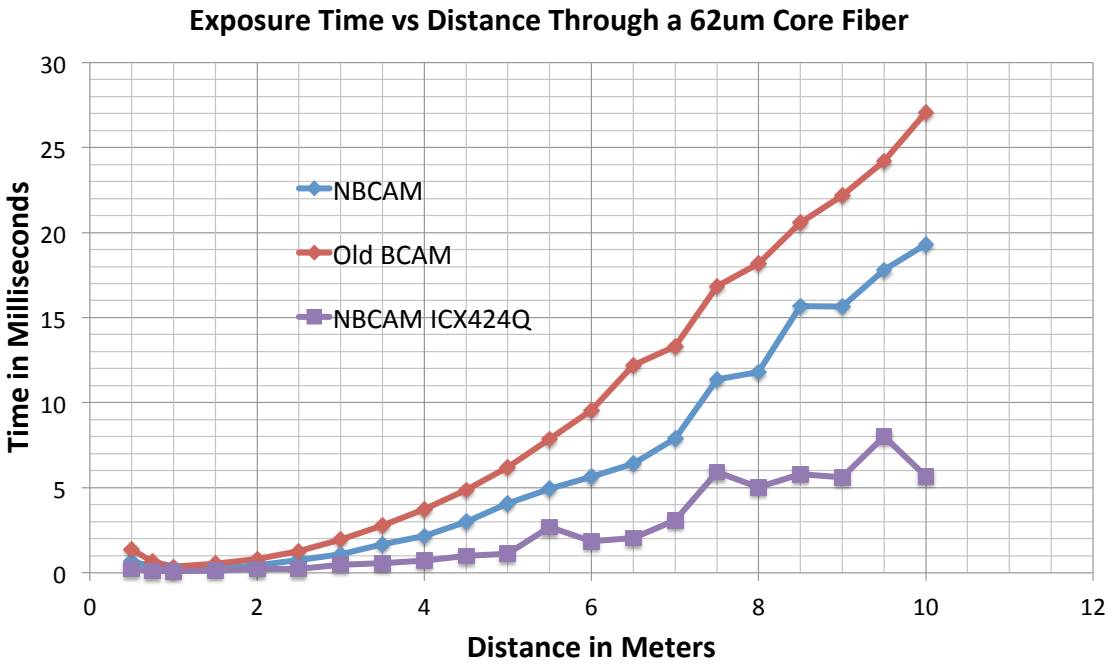

Figure 23: *Pictured are the measured exposure times of an NBCAM and a BCAM viewing light from a Deep Red Luxeon-Z LED driven at 1Amp injected into a* $62.5\mu m$ *fiber at varying distances. The NBCAM was used in both its regular setting and its Q setting. Exposure time was measured as the amount of time to achieve a spot with peak intensity of 170-190 counts.*

the measured exposure times.

I then plotted the $62.5\mu m$ core fiber source values with my estimated exposure time when viewing the fiber source. I then plotted the data with my estimated exposure times with a quantum efficiency of .3 and a charge conversion of $7.68\mu V/electron$. The data lined up well again, showing that my method for approximating the exposure times was fair. The two plots are shown in figure 27 and 28.

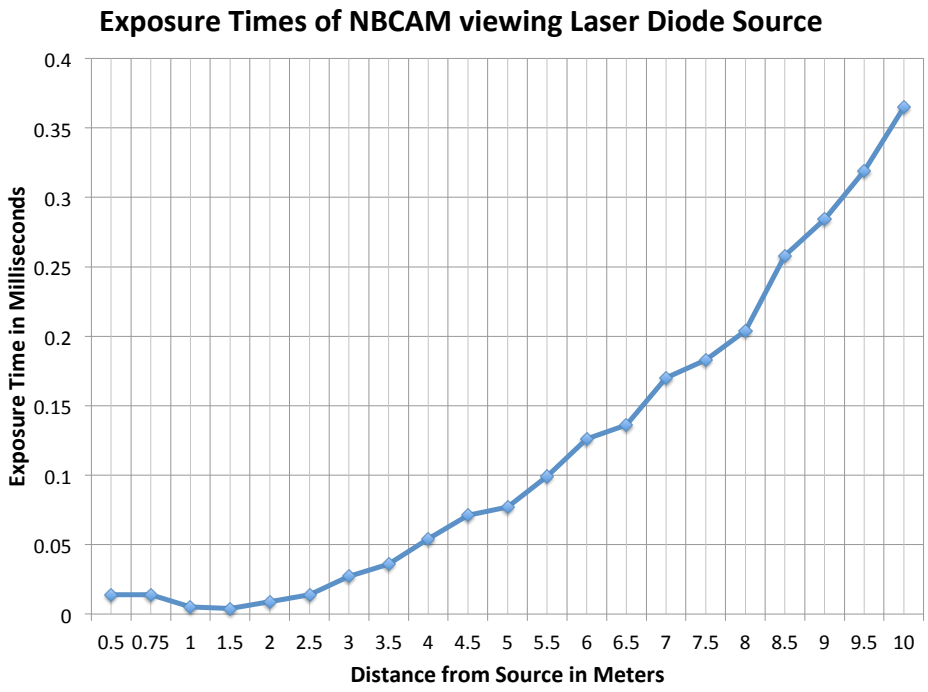

Figure 24: *Pictured are the measured exposure times of an NBCAM viewing light from a laser diode driven by another NBCAM at varying distances. Exposure time was measured as the amount of time to achieve a spot with peak intensity of 180-190 counts.*

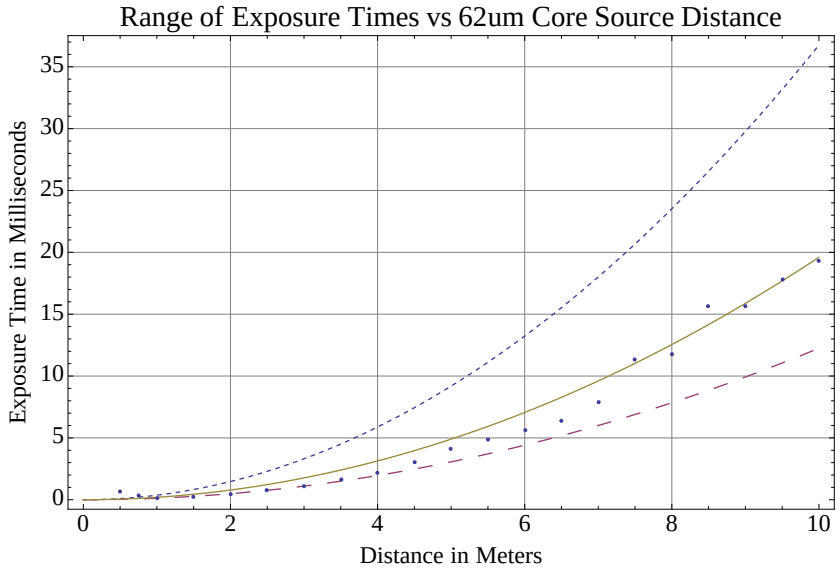

Figure 27: *Pictured are the measured exposure times of an NBCAM viewing light from a Deep Red Luxeon-Z LED driven at* $1Amp$ *injected into a* $62.5\mu m$ *fiber at varying distances as well as the range of estimated exposure times, where the blue line with small dashing, the yellow line no dashing, and the pink line with large dashing represent the same charge conversion and quantum efficiencies as they did in figure 19. Exposure time was measured as the amount of time to achieve a spot with peak intensity of 170-190 counts.*

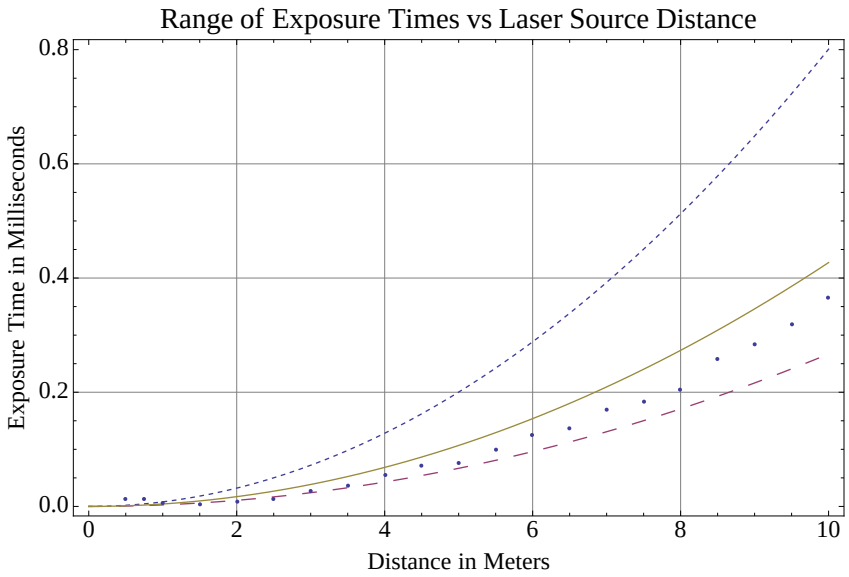

Figure 25: *Pictured are the measured exposure times of an NBCAM viewing light from a laser diode driven by another NBCAM at varying distances as well as the range of estimated exposure times, where the blue line with small dashing, the yellow line no dashing, and the pink line with large dashing represent the same charge conversion and quantum efficiencies as they did in figure 19. Exposure time was measured as the amount of time to achieve a spot with peak intensity of 180-190 counts.*

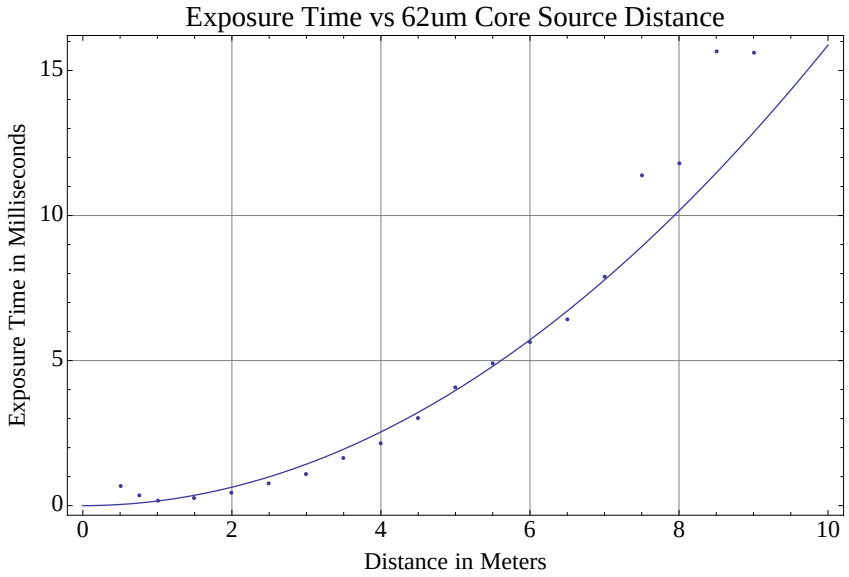

Figure 28: *Pictured are the measured exposure times of an NBCAM viewing light from a Deep Red Luxeon-Z LED driven at 1Amp injected into a* $62.5\mu m$ *fiber at varying distances as well as the estimated exposure times using the fitted charge conversion of* $7.68\mu V/electron$ *and a quantum efficiency of .3. Exposure time was measured as the amount of time to achieve a spot with peak intensity of 170-190 counts.*

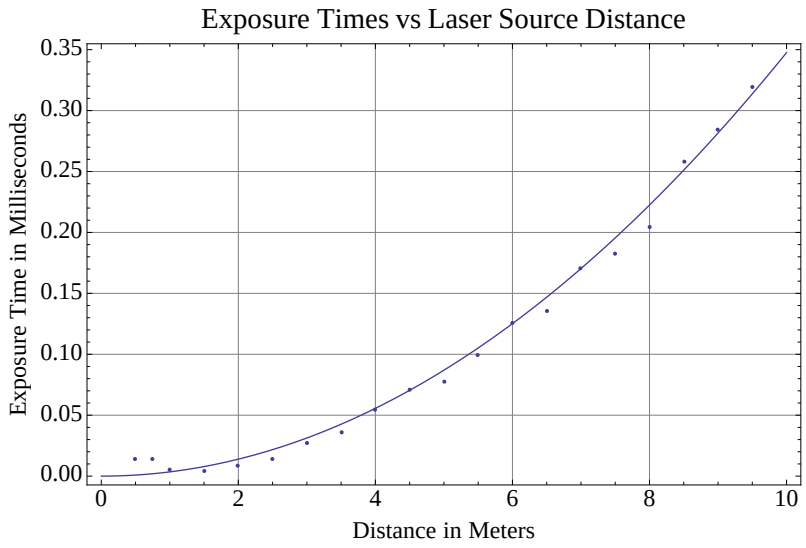

Figure 26: *Pictured are the measured exposure times of an NBCAM viewing light from a laser diode driven by another NBCAM at varying distances as well as the estimated exposure times using the fitted charge conversion of* $7.68\mu V/electron$ *and a quantum efficiency of .3. Exposure time was measured as the amount of time to achieve a spot with peak intensity of 180-190 counts.*

The measured exposure times of the fiber optic source and the laser diode source are not accurately estimated as the source becomes very close to the NBCAM. This is expected, as I assumed a perfect focus which becomes increasingly inaccurate as the NBCAM gets close to the source. The image of the spot spreads across the CCD at close distances, requiring longer exposure times to reach the required peak intensity. The main focus of the estimations were the longest lines for the NBCAM at $3m$, which is also the approximate focus for the NBCAM, since my experimental measurements had shown that the exposure time at $3m$ was longer than the closest spot at $.5m$. There were also inaccuracies in the estimation of the fiber source exposure time at distances greater than $7m$, which may be due to the assumption that the light is centered on a pixel and not on the border of pixels, as well as the source and camera being in a perfect line when moving away. In this regard, the source was very slightly angled and so the spot very slowly moved on the CCD as the separation increased, which may be the source of the loss in smoothness in the plot of exposure times at large separations. The exaggeration of the smoothness loss in the Q setting as shown in figure 23 is support for this idea, as the area of the pixels is quadrupled and so when light would be split between two pixels when the camera is moved it would cause a more dramatic effect than with the smaller pixels. In the fiber source experiment, there was also a larger allowed range of peak intensities than in the laser diode exposure time measurements, so the more jagged line of exposure times may be in part due to the larger range of possible exposure times at each distance.

7.4 RASNIK Mask Exposure Times

In the bar head circuit, the nine Luxeon-Z Royal Blue LEDs are current controlled so that they cannot exceed $70mA$.The voltage drop across them is too great though, so that only $35mA$ can actually be driven through them during operation.[24] I measured the power emitted by the RASNIK mask when being driven by this nine LED array, which I used in my estimation of the exposure time of the RASNIK mask lines. I then measured the exposure times for the two unique lines using a mock alignment bar set up on our optical rail. The exposure times were about $1.1ms$ for the shorter line and $1.3ms$ for the longer line. These were close to my values of $1ms$ and $1.2ms$ respectively when using a charge conversion of $7.68\mu V/electron$ and a quantum efficiency of .39 found from the cameras with the ICX424AL. These values are within 10% of the expected values, which shows that my estimation method is still fairly accurate even when measuring blue light over the entire CCD instead of red light over a few pixels.

8 Total Tolerances

Utilizing both experimental measurements and theoretical predictions, I was able to evaluate the expected tolerance the system would have to neutron and ionizing radiation. As shown by irradiation experiments, most of the electronics in the NSW will be functional after more than an order of magnitude greater radiation than expected, and will not affect the alignment system. The exception to this is that the ICX424AL will have increased dark current, the fiber optic cables will darken, and the Luxeon-Z LEDs will lose power. To understand the effect this will have on the alignment system, I studied how the combination of all three losses after both ionizing and neutron radiation will contribute to the total functionality of the system.

8.1 Light Production as a Function of Radiation

I utilized the fitted charge conversion for the ICX424AL and the total loss in transmission of the Deep Red Luxeon-Z LED's light earlier derived to predict the exposure time for a fiber optic source in the NSW. This is plotted in figure 29, showing exposure time at different distances and transmission coefficients. The main area of interest is the exposure time at $3m$ as transmission drops, since this is the longest line in the NSW and will have the greatest exposure times used in the alignment system. The exposure time at $3m$ as transmission of light drops is plotted in figure 30. The maximum exposure time after $550Gy$ experienced by the fiber and $16Tn$ experienced by the LED is $8.1ms$.

These estimations so far have been ignoring dark current in the CCD, and have been assuming a peak intensity of about 130-150 counts above the background. To include dark current, I estimated the exposure time to only create a 30 count increase above the background. Using this, I could then estimate the amount of radiation tolerance we would have as the amount of radiation we can endure before the background increases to 225 counts in the time it would take for a 30 count intensity image.

In order to increase ionizing and neutron radiation in the system until the background

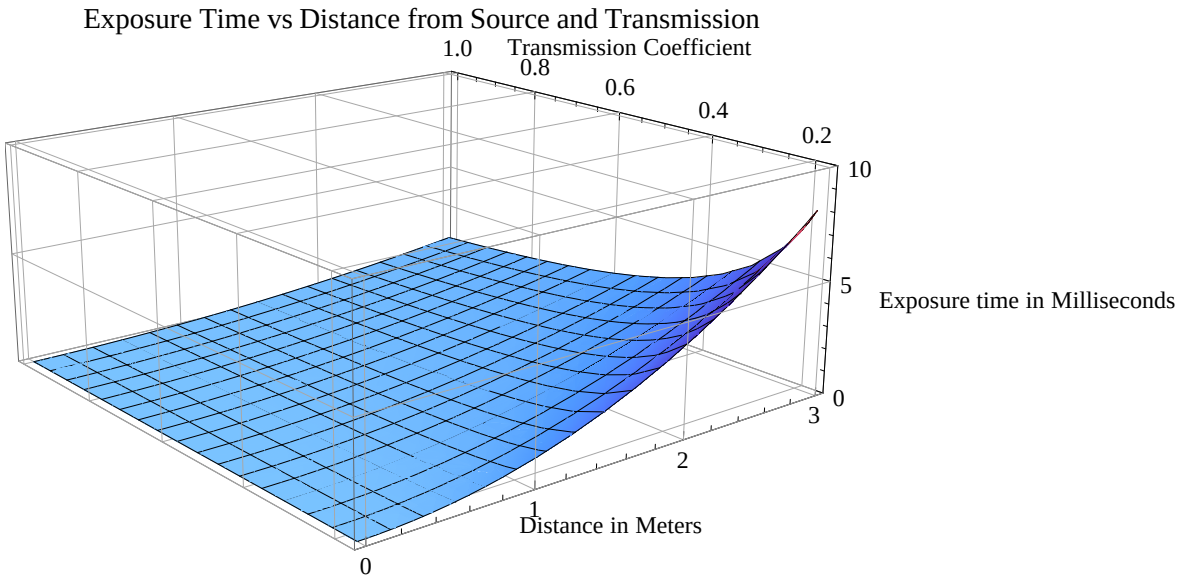

Figure 29: *Pictured are the estimated exposure times of an NBCAM viewing light from a Deep Red Luxeon-Z LED driven at* $1Amp$ *injected into a* $62.5\mu m$ *fiber at varying distances as well as varying transmission coefficients. Exposure time was measured as the amount of time to achieve a spot with peak intensity of 170-190 counts.*

is 30 counts for the longest exposure time source, I needed to represent the damage to the different components as continuous functions. I was able to fit a function to the Draka fiber darkening due to having many data points for the transmittance versus ionizing radiation. For the LEDs, we only had two irradiated power values. To represent the power loss as a continuous function, I had to assume the Luxeon-Z LEDs lost power following the same function as the LEDs we have worked with in the past. In the past, we have found that LEDs lose power as a geometric function of the radiation. We have modeled the power emitted as an exponential decay whose exponent is linear with neutron radiation dose. Using this model and the measured power loss of the LEDs at 16Tn I was able to create a function to estimate the power of the Luxeon-Z LEDs at varying neutron radiation doses.

8.2 Dark Current on the CCD

Having a continuous model for the light reaching the CCD that includes radiation levels and a function to show the exposure time for a given amount of light reaching the CCD, I only needed to combine the models describing the effect ionizing and neutron radiation had on the CCD to then determine the total tolerance to radiation of the light imaging systems.

Ionizing radiation increases the dark current background intensity linearly with exposure time and with time spent in the transfer area. This can be broken into two functions for imaging a spot, one independent of the spot's exposure time and one dependent on it. These two functions are $.111 counts/row/475Gy = .234 counts/row/kGy$ and $15 counts/ms/kGy$. There are 504 rows in the CCD, so we can use the dark current increase in the last row to be the worst effect on the CCD. This would give an intensity function at the bottom row for a $0ms$ exposure of $117.777 counts/kGy$, while the exposure time dependent function would

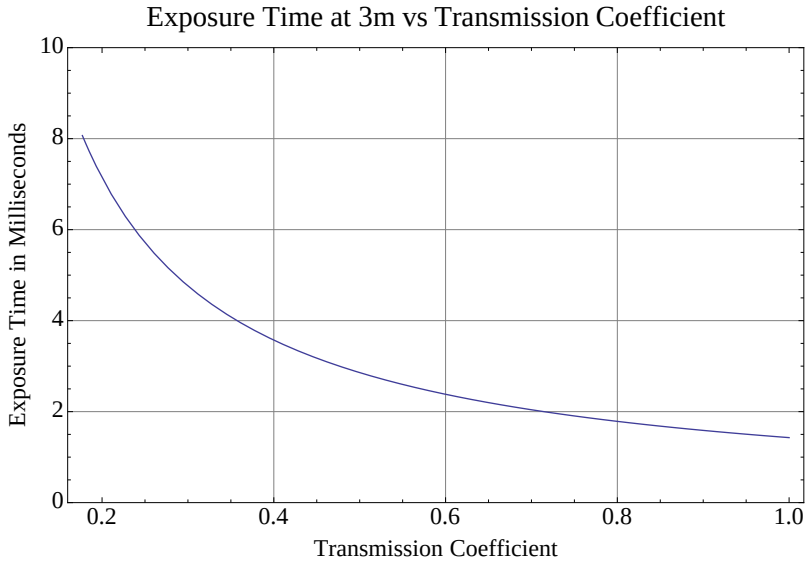

Figure 30: *Pictured are the estimated exposure times of an NBCAM viewing light from a Deep Red Luxeon-Z LED driven at* $1Amp$ *injected into a* $62.5\mu m$ *fiber at* $3m$ *from the source, with varying transmission coefficients. Exposure time was measured as the amount of time to achieve a spot with peak intensity of 170-190 counts.*

remain unchanged.

Neutron radiation also linearly increases the background intensity for the exposure time dependent portion and the transfer time dependent portion. Using the transfer time as $180ms$[27] we can use the function of $10.44counts/Tn$ for the transfer portion of the radiation damage, and then the exposure time dependent portion is $.115counts/ms/Tn$. Both the ionizing and neutron radiation transfer damage functions assume the CCD is reading out the entire image at once, though with software changes we can read out half an image at a time and reduce the transfer time by a factor of two if necessary, which would reduce the transfer area damage by a factor of 2.[27] We will avoid that for now, and assume we will have a large enough safety factor without more complicated software implementations.

The CCD is expected to receive at the worst radius $3.5Tn$ and $70Gy$. Using this, we can write the radiation damage in terms of a single factor of expected doses instead of two different radiation levels. This is simply replacing Gy with (1/70)F and Tn with (1/3.5)F in the CCD, where F stands for factor of the expected dose. This reduces the four background intensity increase functions to two functions of F, one also dependent on the exposure time and one only dependent on F. These two functions are $48.93counts/F$ for the transfer area intensity increase and $1.45counts/ms/F$ for the exposure time depended intensity increase. Using this I can replace Gy and Tn with F in the exposure time functions and then find the maximum value of F such that the background intensity is less than 225 counts. The plot of exposure time for a 30 count spot with increasing factor when viewing the fiber optic source is shown in figure 31.

Using the formulas for the background intensity increase, the exposure time for a 30 count spot, and the constant 40 count pedestal I was able to find that the maximum factor value is 3.7, where any higher levels of radiation we cannot create a 30 count spot above the

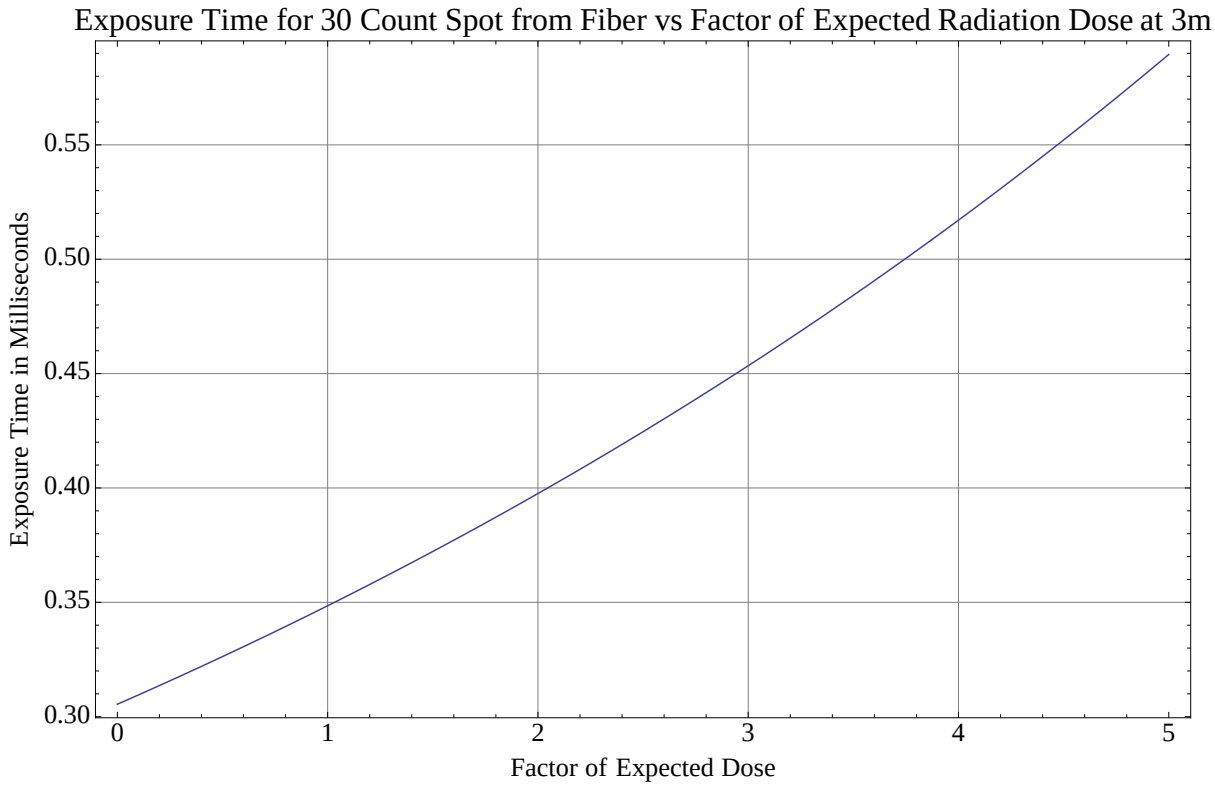

Figure 31: *Pictured are the estimated exposure times of an NBCAM viewing light from a Deep Red Luxeon-Z LED driven at* $1Amp$ *injected into a* $62.5\mu m$ *fiber at* $3m$ *from the source, with increasing factor of expected dose. Exposure time was measured as the amount of time to achieve a spot with peak intensity of 30 counts above the background.*

background. Our safety factor to simultaneous ionizing and neutron radiation therefore is 3.7. Lowering the spot to 15 counts above the background would increase the safety factor to above 4, though I have not done this since I have been assuming a single image is taken for each analysis. To lower the image count to 15 above the background would require taking more than one image of the spot, to increase the resolution to the required $400nm$. This can be very simply done in software, so it is important to note that if this is done the safety factor would increase to 4.

8.3 Ionizing and Neutron Separate Tolerances

It can also be of interest what the tolerance of the system is to specifically ionizing radiation or neutron radiation. To determine the safety factor of tolerance to ionizing radiation, I can use the same formulas as before but with the neutron radiation effects ignored. The increase in the background intensity that's dependent on exposure time becomes simply $1.024counts/ms/F$ and the increase due to the transferring the image becomes $12.44counts/F$. The power loss in the LED can be ignored due to it being solely an effect of neutron radiation, so transmission drop is only due to the Draka fiber losing transmittance in ionizing radiation. Using this in the exposure time equations, I get a maximum factor of

14 for ionizing radiation, so we have a safety factor of 14 to ionizing radiation if we ignore neutron radiation.

To get the safety factor for neutron radiation, I can ignore the fiber transmission loss. The intensity increase equations become $36.54 counts/F$ and $.403 counts/ms/F$. Utilizing the exposure time equations and ignoring the fiber transmission loss component, I get a maximum factor of 5, so we have a safety factor of 5 to neutron radiation if we ignore ionizing radiation. This shows that we are more tolerant to ionizing radiation than neutron radiation by almost a factor of three. A table to summarize these results is shown in figure 32.

Dose Factor	Fiber Dose	CCD Dose	LED Dose	Fiber Transmission	LED Power	Exposure Time(ms)	Dark Current(counts)
1 (Both)	55Gy/2.35Tn	70Gy/3.5Tn	40Gy/1.2Tn	97.25%	90.12%	0.35	49
3.7 (Both)	203Gy/8.7Tn	259Gy/13Tn	148Gy/4.44Tn	90.28%	68.06%	0.5	184
4 (Both)	220Gy/9.4Tn	280Gy/14Tn	160Gy/4.6Tn	89.54%	65.97%	0.52	199
1 (Neutron)	0Gy/2.35Tn	0Gy/3.5Tn	0Gy/1.2Tn	100%	90.12%	0.34	37
5 (Neutron)	0Gy/11.75Tn	0Gy/17.5Tn	0Gy/6Tn	100%	59.46%	0.51	184
1 (Ionizing)	55Gy/0Tn	70Gy/0Tn	40Gy/0Tn	97.25%	100%	0.31	13
14 (Ionizing)	770Gy/0Tn	980Gy/0Tn	560Gy/0Tn	69.01%	100%	0.44	181

Figure 32: *Pictured are the overall results for the different safety factors of radiation. It shows the radiation levels for each relevant component, fiber optic cable's transmission percent, the LED's power percent, the exposure time for a 30 count spot, and the dark current background for different factors of expected radiation doses. This is only for the fiber optic imaging line at $3m$ since this is the most vulnerable to radiation portion of the system, so these safety factors extend to the entire system.*

9 Conclusion and Future Work

The alignment system for the NSW utilizes several imaging techniques and temperature measurements to create a coordinate system in the muon spectrometer, and connect the chamber coordinate systems to the ATLAS global coordinate system. Due to the increased luminosity after an upgrade at the LHC, the Small Wheel at ATLAS will need to be replaced with the NSW to be able to operate properly in the increases background cavern radiation environment. The alignment system components must be updated and survive in this increased radiation environment.

The temperature measuring circuits contain mosfets which will operate at $2kGy$, while no other components of their circuits lose functionality below $2kGy$. The temperature circuits are not affected by neutron radiation at an order of magnitude above the expected doses

as far as our tests have shown, though further testing can be done to confirm the lack of neutron damage by going beyond an order of magnitude of neutron radiation. As of now, the temperature measurement system in the NSW has a safety factor of at least 10 to radiation.

The imaging for the NSW uses the ICX424AL CCD for all imaging lines. The three forms of imaging are RASNIK mask imaging, laser diode imaging, and fiber optic source imaging. The RASNIK mask and fiber optic source imaging are the only ones affected by radiation other than in the CCD, and the fiber optic source is affected more severely. To consider the maximum tolerance to radiation, only the fiber source needs to be considered since for any level the fiber source is functioning, the other imaging lines are also functioning.

The CCD's background intensity increases with radiation, and also has an exposure time dependent increase in background intensity after radiation. The maximum factor of simultaneous neutron and ionizing radiation the fiber optic line can function under is a factor of 3.7, which is our safety factor. It can endure a safety factor of 14 ionizing radiation if there is no neutron radiation, or a safety factor of 5 neutron radiation is there is no ionizing radiation. Since the fiber optic line is the most affected portion of the alignment system by radiation, these safety factors extend to the system as a whole.

The entire alignment system has not been fully tested under ionizing and neutron radiation, but instead components and some full circuits have been tested. In the future, we will need to test each circuit in its entirety up to at least a factor of 5 more ionizing and neutron radiation, though ideally up to a factor of 10 more. This includes the NBCAM, the Multiplexer, the repeater, and the injector. The bar head has been fully tested in both environments. Each of these, including the bar head, should then be tested after being irradiated in both environments to see if there are any issues that are not noticeable under each irradiation experiment separately but combine to a significant effect.

The fiber optic imaging assumes the LED is able to be driven at $1Amp$ in the injector circuit. This assumes proper heat sinking. The injector has not been fully designed yet, so I was not able to test that we are able to achieve this current with the actual injector. The injector must be designed with heat sinking in mind so that we can get the highest current possible. If we are able to get a higher current with better heat sinking it can only improve the system.

The loss or increase in light will not drastically affect the overall safety factor, as the main issue with radiation comes from the increase in the intensity in the CCD when transferring the image out of the CCD as discussed previously. This issue can be improved by changing the current software to allow the splitting of the image and then stitching together of two images. The CCD allows us to take and read out half the image at a time, which would reduce the intensity increase in the transfer area by a factor of two. This would nearly double the safety factor for the system. This would require more complicated software implementation, but can be done if the current safety factor is deemed too low,

Overall, the current design for the NSW alignment system has a total safety factor of 3.7 to radiation. We can implement more sophisticated software to increase this to almost 8, by splitting the image in two and reading out half images at a time, and also taking multiple images of a spot to lower the needed intensity above the background. This safety factor is pending future irradiation experiments on all NSW alignment circuits in their entirety, as well as completion of all of the circuits. As of now, there is nothing to indicate that we will encounter any loss in functionality up to a factor of 3.7 more radiation than expected in the

NSW.

References

[1] Cian O'Luanaigh, "The Large Hadron Collider", *CERN*, 21 Jan. 2014, http://home.cern/topics/large-hadron-collider.

[2] Cian O'Luanaigh, "ATLAS", *CERN*, 08 Feb. 2012, http://home.cern/about/experiments/atlas.

[3] "The Inner Detector", *ATLAS*, http://atlas.cern/discover/detector/inner-detector.

[4] "The Calorimeter", *ATLAS*, http://www.atlas.ch/calorimeter.html.

[5] "Atlas Detector", *SCIPP University of California Santa Barbara*, http://scipp.ucsc.edu/personnel/atlasdet.jpg.

[6] "ATLAS Muon Spectrometer Technical Design Report", *ATLAS Muon Collaboration*, CERN report, CERN/LHCC/97-22.

[7] "ATLAS Muon', *IRFU*, 08 Jan. 2015, http://irfu.cea.fr/Phocea/Vie_des_labos/Ast/ast_sstechnique.php?id_ast=387.

[8] A Zibell, "Micromegas Detectors for the Upgrade of the ATLAS Muon Spectrometer", *IOPscience* 9, 20 Aug. 2014, http://iopscience.iop.org/article/10.1088/1748-0221/9/08/C08013/meta.

[9] Kevan Hashemi, "Irradiation Apparatus", *Brandeis University High Energy Physics Electronics Shop*, 2012-2016, http://alignment.hep.brandeis.edu/Irradiation/Apparatus.html.

[10] Christoph Amelung et al., "The Optical Alignment System of the ATLAS Muon Spectrometer Endcaps", *Brandeis University High Energy Physics Electronics Shop*, 28 Mar. 2008, http://alignment.hep.brandeis.edu/ATLAS/ECA.pdf.

[11] Kevan Hashemi, "Alignment Electronics for the New Small Wheel", *Brandeis University High Energy Physics Electronics Shop*, 12 Mar. 2015, http://alignment.hep.brandeis.edu/ATLAS/2015_MAR_CERN/Index.html.

[12] Richard Studley, "nSW In-Bar Alignment Production Manual", *Brandeis University High Energy Physics Electronics Shop* 06 Mar. 2015, http://alignment.hep.brandeis.edu/Devices/Alignment_Bar/nSW_Alignment_Bar/nSW_In_Bar_Alignment.html.

[13] Andrey Dushkin, "NSW Alignment Layout Alignment Bars and BCAMs Design", *Indico*, 12 Mar. 2015, https://indico.cern.ch/event/375608/contributions/1798024/attachments/748642/1027037/NSW_layout.pdf.

[14] "piece v", *NIKHEF*, http://www.nikhef.nl/pub/departments/et/experiments/atlas/rasnik/atlas_rasnik/rasled/piece_v.gif.

[15] Kevan Hashemi, "BCAM User Manual", *Brandeis University High Energy Physics Electronics Shop*, 2002-2015, http://alignment.hep.brandeis.edu/Devices/BCAM/User_Manual.html.

[16] Craig Blocker, "nSW Alignment Overview", *Indico*, 12 Mar. 2015, https://indico.cern.ch/event/375608/contributions/1798021/attachments/748639/1027034/CERN_NSW_Alignment_review_March_12_2015.pdf.

[17] Kevan Hashemi, "Contact Injector (A2080) Manual", *Brandeis University High Energy Physics Electronics Shop*, 2014-2016, http://alignment.hep.brandeis.edu/Electronics/A2080/M2080.html.

[18] Kevan Hashemi, "LWDAQ User Manual", *Brandeis University High Energy Physics Electronics Shop*, 12 Mar. 2015, http://alignment.hep.brandeis.edu/Electronics/LWDAQ/Manual.html.

[19] "Ionizing Radiation", *Bodner Research Web*, http://chemed.chem.purdue.edu/genchem/topicreview/bp/ch23/radiation.php.

[20] Kevan Hashemi, "Irradiation Tests", *Brandeis University High Energy Physics Electronics Shop*, 2013-2016, http://alignment.hep.brandeis.edu/Irradiation/Tests.html.

[21] R. Nave, "The Interaction of Radiation with Matter", *Hyper Physics*, http://hyperphysics.phy-astr.gsu.edu/hbase/mod3.html.

[22] "MOSFET N CHANNEL", *Telespares*, http://www.telespares.com.au/index.php?main_page=product_info&cPath=45323_45373&products_id$\bar{3}$19423.

[23] "MOSFET as a Switch", *ElectronicsTutorials*, http://www.electronics-tutorials.ws/transistor/tran_7.html.

[24] Kevan Hashemi, "Bar Head (A2082) Manual", *Brandeis University High Energy Physics Electronics Shop*, 2015, http://alignment.hep.brandeis.edu/Electronics/A2082/M2082.html.

[25] "2 Fiber Tight Buffer Zipcord Cable - OFNR/FT4", *Brandeis University High Energy Physics Electronics Shop*, http://alignment.hep.brandeis.edu/Electronics/Data/S705T-02F-62N3.pdf.

[26] Kevan Hashemi & James Bensinger, "Irradiation of the TC255 CCD by Fast Neutrons", http://alignment.hep.brandeis.edu/ATLAS/MUON-98-253.pdf.

[27] Richard Studley, "Irradiation of nSW Upgrade Components by Fast Neutrons", *Brandeis University High Energy Physics Electronics Shop* 06 Mar. 2015, http://alignment.hep.brandeis.edu/Irradiation/Lowell_2014/Irradiation_Of_nSW_Upgrade_Electronics_By_Fast_Neutrons.pdf.

[28] "Types of Ionizing Radiation", *Mirion Technologies*, https://www.mirion.com/introduction-to-radiation-safety/types-of-ionizing-radiation/.

[29] Keith Holbert "Radiation Effects and Damage", *Arizona State University*, http://holbert.faculty.asu.edu/eee560/RadiationEffectsDamage.pdf.

[30] "Mako G-032", *Allied Vision*, https://www.alliedvision.com/en/products/cameras/detail/Mako%20G/G-032.html.

[31] Chris McFee, "An introduction to CCD operation", *Mullard Space Science Laboratory*, http://www.mssl.ucl.ac.uk/www_detector/optheory/ccdoperation.html.

[32] "AIGaInP Visible Laser Diode", *Brandeis University High Energy Physics Electronics Shop*, http://alignment.hep.brandeis.edu/Electronics/Data/ADL65055TL.pdf.

[33] "Luxeon Z", *Brandeis University High Energy Physics Electronics Shop*, http://alignment.hep.brandeis.edu/Electronics/Data/Luxeon_Z.pdf.

[34] "Ultra WF Series – WF 100/110 P 37", *Engineering 360*, http://datasheets.globalspec.com/ds/1208/CeramOptec/5986BF98-581E-4EC9-A2C3-410E54F3CF67.